Alma Mater Studiorum - Università di Bologna

SCUOLA DI SCIENZE

Dipartimento di Chimica Industriale "Toso Montanari"

Corso di Laurea Magistrale in

Chimica Industriale

Classe LM-71 - Scienze e Tecnologie della Chimica Industriale

Late Transition Metal-Oxo complexes: Synthesis, and Biorelevant Reactivity

Tesi di laurea sperimentale

CANDIDATO

Chiara Cecchini

RELATORE

Chiar.mo Prof. Stefano Zacchini

CORRELATORI

Dr. Aidan McDonald

Ph.D Paolo Pirovano

Anno Accademico 2015-2016

Abstract

High-valent terminal metal-oxygen adducts are supposed to be potent oxidising intermediates in enzymatic catalyses. In contrast to those from groups 6-8, oxidants that contain late transition metals (Co, Ni, Cu) are poorly understood. Because of their high reactivity, only a few examples of these compounds have been observed.

The aim of this project was to investigate the reactivity of high-valent Ni(III) complexes, containing a monodentate oxygen-donor ligands, in hydrogen atom abstraction (HAA) and oxygen atom transfer (OAT) reactions which are typical of biological high-valent metal-oxygen species. Particularly, the Ni(III) complexes were generated in situ, at low temperature, from the oxidation of the Ni(II) species.

The nickel complexes studied during this work were supported by tridentate ligands, with a strong σ-donating ability and exceedingly resistant to several common degradation pathways. These complexes vary based on the monodentate group in the fourth coordination position site, which can be neutral or anionic.

In particular, we prepared four different Ni(III) complexes $[Ni^{III}(pyN_2^{Me2})(OCO_2H)]$ (**12**), $[Ni^{III}(pyN_2^{Me2})(ONO_2)]$ (**14**), $[Ni^{III}(pyN_2^{Me2})(OC(O)CH_3)]$ (**18**) and $[Ni^{III}(pyN_2^{Me2})(OC(O)H)]$ (**25**). They feature a bicarbonate ($-OCO_2H$), nitrate ($-ONO_2$), acetate ($-OC(O)CH_3$) and formate (-OC(O)H) group, respectively.

HAA and OAT reactions were performed by adding 2,6-di-tert-butylphenol (2,6-DTBP) at -40 °C, and triphenylphosphine (PPh_3) at -80 °C, to the in situ generated Ni(III) complexes, respectively. These reactions were carried out by adding 7 to 500 equivalents of substrate, in order to ensure pseudo-first order conditions. Since, the reactivity of the Ni(III) complex featured by the bicarbonate group has been studied in a previous work, we only investigated that of the species bearing the nitrate, acetate and formate ligand. Finally we compared the value of the reaction rate of all the four species in the HAA and OAT reactions.

Riassunto

I complessi dei metalli di transizione in alto stato di ossidazione, caratterizzati da leganti O-donatori, sono ritenuti potenti ossidanti in catalisi enzimatica. In questo campo i complessi di Co, Ni, Cu sono meno conosciuti rispetto a quelli dei metalli di transizione del gruppo 6-8, perché altamente reattivi e quindi più difficilmente isolabili.

Lo scopo di questo lavoro di tesi è stato quello di studiare la reattività di complessi di Ni(III) contenenti leganti monodentati O-donatori coordinati al centro metallico nel quarto sito di coordinazione. In particolare, è stata valutata la reattività di questi complessi nelle reazioni di OAT e HAA, che coinvolgono il trasferimento di un atomo di ossigeno e l'estrazione di un atomo di idrogeno rispettivamente. I complessi di Ni(III) sono stati ottenuti in situ mediante l'ossidazione di complessi di Ni(II), e differiscono tra loro in base al sostituente monodentato (neutro od anionico) presente sul quarto sito di coordinazione. I restanti tre siti di coordinazione, risultano occupati da un legante tridentato sigma donatore, estremamente resistente a diversi processi di degradazione.

Complessivamente, sono stati preparati quattro complessi di Ni(III): $[Ni^{III}(pyN_2^{Me2})(OCO_2H)]$ (**12**), $[Ni^{III}(pyN_2^{Me2})(ONO_2)]$ (**14**), $[Ni^{III}(pyN_2^{Me2})(OC(O)CH_3)]$ (**18**) e $[Ni^{III}(pyN_2^{Me2})(OC(O)H)]$ (**25**), caratterizzati dalla presenza di un gruppo monodentato bicarbonato ($-OCO_2H$), nitrato ($-ONO_2$), acetato ($-OC(O)CH_3$) e formiato (-OC(O)H) rispettivamente.

Le reazioni di HAA e OAT sono state realizzate facendo reagire i complessi di Ni(III), generati in situ, con 2,6-di-ter-butilfenolo (2,6-DTBP) a - 40 °C, e trifenilfosfina (PPh_3) a - 80 °C rispettivamente.

Durante le reazioni, il substrato (2,6-DTBP o PPh_3) è stato aggiunto in largo eccesso (7-500 equivalenti) in modo da assicurare una cinetica di pseudo primo ordine.

Dato che la reattività del complesso di Ni(III) con il gruppo bicarbonato, era già stata esaminata in un lavoro precedente, abbiamo studiato la velocità di reazione per i complessi contenenti il gruppo nitrato, acetato e formiato ed infine confrontato i valori di tutte e quattro le specie.

Acknowledgements

I would like to express my appreciation for all the people who helped me during my thesis work. I would like to express my gratitude to Dr. Aidan McDonald for giving me the opportunity to join his group and for his willingness. I'm also grateful to my supervisor Professor Stefano Zacchini for his encouragement in applying for the Erasmus program and his assistance in writing the thesis. I would also like to thank Ph.D Paolo Pirovano, who, for his expertise and patience, helped me a lot during my internship.
Finally I want to thank my family who have always supported me during all my studies.

Abbreviations

buea Tris[(N'-tertbutylureaylato)-N-ethyl)]aminato

CAN Ammonium cerium(IV) nitrate

DMF N,N-Dimethylformamide

DTPB 2,6-Ditertbutylphenol

EPR Electron paramagnetic resonance

ET Electron transfer

HAA Hydrogen atom abstraction

mCPBA 3-Chloroperbenzoic acid

Magic Blue Tris(4-bromophenyl)ammoniumyl hexachloroantimonate

OAT Oxygen atom transfer

PCET Proton-coupled electron transfer

PT Proton transfer

pyN_2^{iPr2} N,N'-Bis(2,6-diisopropylphenyl)-2,6-pyridinedicarboxamidate

pyN_2^{Me2} N,N'-Bis(2,6-dimethylphenyl)-2,6-pyridinedicarboxamidate

pyN_2^{R2} N,N'-Bis(2,6-R-phenyl)-2,6-pyridinedicarboxamidate

TAML Tetraamidomacrocyclic ligand

TEMPO (2,2,6,6-Tetramethyl-piperidin-1-yl)oxyl

THF Tetrahydrofuran

TMC Tetramethylcyclam

This thesis work has been carried out during the Erasmus exchange period in the ''*Bioinspired Inorganic Chemistry* (BIC) *group''* led by Dr. Aidan McDonald based in the School of Chemistry at Trinity College Dublin, the University of Dublin. It has been carried out under the supervision of Dr. Aidan McDonald and Ph.D candidate Paolo Pirovano.

Contents

1. Introduction

1.1 The oxidation of hydrocarbons

The selective oxidation of organic molecules is fundamentally important in industry ranging from fine chemicals to commodities production.[1] The main challenge is to make such processes environmentally friendly by employing inexpensive non-polluting reagents and milder conditions. Energy-efficient catalytic methods utilizing atmospheric dioxygen and hydrogen peroxide would be in this sense very attractive. Particularly, industrial interest in the catalytic use of molecular oxygen has always been great because of free of cost air. One major obstacle is related to dioxygen's inertness which contrasts its great oxidizing power. Indeed, since O_2 molecule is paramagnetic with a triplet ground state, a direct combination with organic compounds (singlet molecules) is spin-forbidden. This is the reason why organic matter may exist in the oxygen-rich atmosphere. A class of substrates of great interest in selective oxidation reactions is represented by hydrocarbons. Especially, the development of processes for selective alkanes oxidation is a goal that has long been pursued. In this case, the main issue to overcome is related to the chemical inertness of the C–H bond that hampers the conversion of alkanes into higher-valent products.[2] Indeed, harsh conditions are required in these transformations leading to energy-intensive and poorly selective processes. For example, endothermic processes such as cracking and thermal dehydrogenation convert alkanes to valuable olefins, but they require high temperatures and pressures. On the other hand, the currently prevalent use of alkanes in combustion applications exploits their energy content, but not their considerable potential as valuable precursors for more important and expensive chemicals. Indeed such reactions are not readily controllable and usually proceed to the thermodynamically stable and economically unattractive products, carbon dioxide and water. Alkane chemistry could also improve the utilization of methane, the principal component of natural gas, that is expected to play an increasing role in the make-up of energy sources in the near future. Nonetheless, many of the world's established natural gas resource locations are remote, in sites where there is little or no local demand, such as the north slope of Alaska. Moreover, exploitation of such resources is complicated by its gaseous state that hamper the storage and transportation

processes. For this reason, developing efficient strategies for the direct conversion of methane to methanol or other liquid fuels or chemicals could thus significantly improve methane utilization. Overall, the design of new selective oxidation catalysts can lead to important benefits both in economic and environmental field. Particularly, it can allow us to exploit Earth's alkane resources more efficiently and cleanly.[3] The main challenge to overcome is represented by the activation both of the dioxygen molecule and the inert substrates under mild conditions.

1.2 Oxidations in biology

One of the most promising approaches to the design of catalysts capable of the selective oxidation of alkanes is the emulation of biological systems.[4] A variety of metalloenzymes have been shown to perform numerous oxidative reactions including the hydroxylation of inert C-H bond. These processes are highly selective and occur at physiological temperatures and pressures. Therefore, ''bioinspired'' catalysts operating under mild conditions with a moderate energy input, may offer notable rewards from an energetic and economic point of view. Industrial applications of such catalytic systems can be promoted by the abundance in the geosphere and limited toxicity of the metals at the enzymes' active sites: mainly iron and copper. The combination of dioxygen with these paramagnetic metal centres is spin-allowed and leads to the formation of a metal-oxygen species. Such compounds are very reactive but at the same time highly selective towards the substrates. As a result, over the last few decades great efforts have been spent on determining the mechanisms of dioxygen activation in a number of heme and non-heme monooxygenase enzymes containing mononuclear and homo and heterodinuclear active sites. Despite the variety of the enzymes's active sites, a common mechanistic pathway for dioxygen activation has been postulated (Figure 1).[4,5] During the first step, the dioxygen molecule binds to the metal center, undergoes to one-electron reduction and leads to the formation of a metal-superoxo species (O_2^-). In this way, the inert triplet ground state of the dioxygen molecule is converted to a more reactive doublet state of (O_2^-). Subsequently, the superoxo picks up an electron resulting in the formation of a peroxo species, which by addition of a proton, gives a hydroperoxo intermediate. In the final step the latter undergoes O−O bond cleavage and yields a high-valent metal−oxo

species. Otherwise, the superoxo species can abstract a hydrogen atom from the substrate, and form the hydroperoxo species. Regarding the dinuclear species, the corresponding intermediates are peroxo-bridged $M(O_2^-)M$, and oxo-bridged high-valent $M_2(\mu\text{-}O)_2$ species. These metallo-enzymes can act in cooperation with different reducing agents such as NADPH, flavins and iron-sulfur proteins.[6] Nonetheless, if the substrate undergoes a 4-electron oxidation no cofactor is required during the reaction. Despite the ability of superoxo, peroxo and hydroperoxo species, to carry out the direct attack of certain substrates, oxo intermediates are supposed to be the principal reactive species that perform substrate activation.

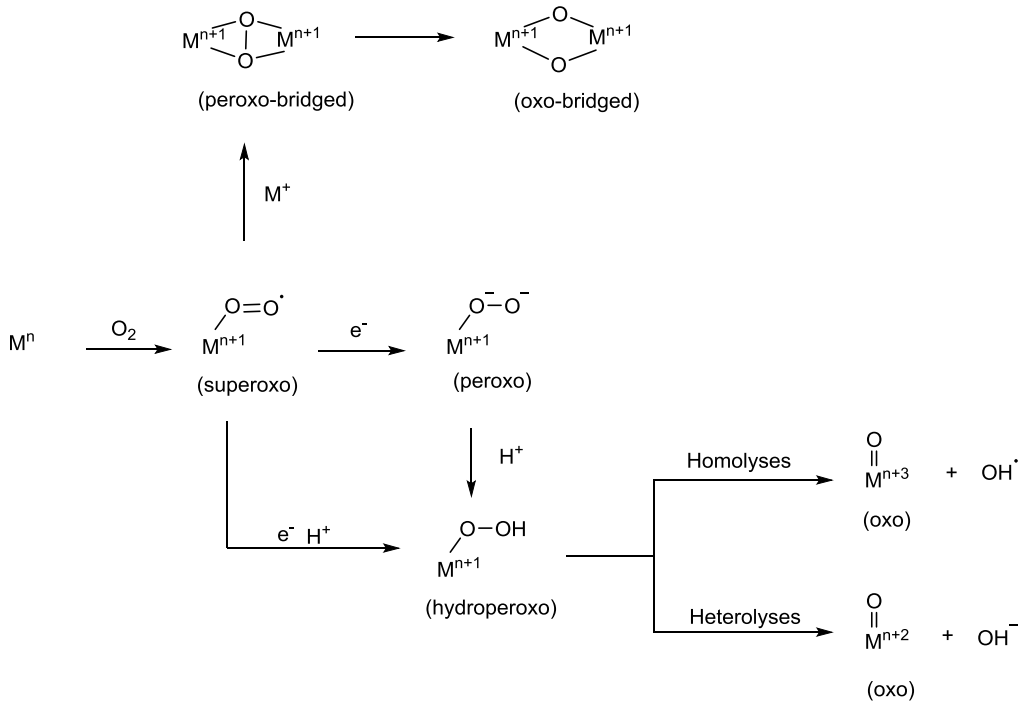

Figure 1. Dioxygen activation and generation of high-valent intermediates in enzymatic oxidation

Several biological oxidations, such as sulfoxidation, N-oxidation and alkene epoxidation, involve the transfer of an oxygen atom (OAT) to an electron-rich substrate. On the other hand the hydrocarbon oxidation reactions (*i.e*. aliphatic hydroxylation, oxidative dehydrogenation, N/O- dealkylation), are initiated by an electrophilic hydrogen atom abstraction (HAA) mechanism (Figure 2a).[7-9] This elementary step involves the concerted transfer of a proton and an electron from the substrate to the oxidant; because the two particles can be transferred to different acceptors within the oxidant structure (*i.e*. the

metal centre and the oxygen ligand), the broader definition of proton-coupled electron transfer (PCET) is sometimes used (Figure 2 b).[10]

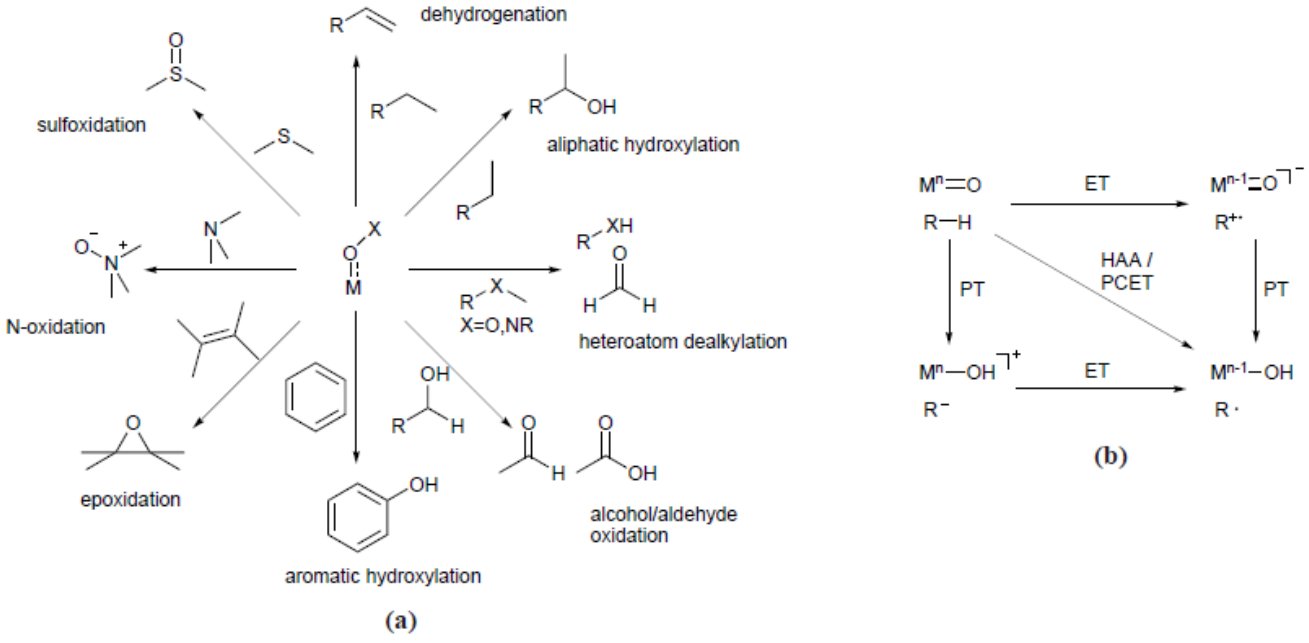

Figure 2. (a) Biological oxidation reactions mediated by matallo-enzymes. **(b)** Relationships between HAA, ET, PT and the intermediates involved. ET = electron transfer;

Among monooxygenases, the superfamily of cytochrome P450 has been the most extensively studied. This superfamily includes a great variety of enzymes, which play an essential role in the metabolism of endogenous substances (e.g steroids) and in the transformation of external substances (xenobiotics) in animals, plants and microorganism (Table 1). In most cases, the reactions catalyzed by P450 enzymes involves reduction of dioxygen, with incorporation of one oxygen atom into the substrate and reduction of the other to water (Figure 3).[11]

$$O_2 + 2\,e^- + 2\,H^+ + Sub \xrightarrow{P\ 450} H_2O + Sub(O)$$

Figure 3. Reaction catalyzed by P450 enzymes

Reaction type	Simplified example	Typical substrate
Aliphatic hydroxylation	cyclohexane ⟶ cyclohexanol	Pentobarbital
Aromatic hydroxylation	benzene ⟶ phenol	Phenobarbital
Alkene epoxidation	Cyclohexene ⟶ Cyclohexene oxide	Aldrin
N-dealkylation	$CH_3N(H)CH_3$ ⟶ $CH_3NH_2 + H_2C{=}O$	Methadone
O-dealkylation	$C_6H_5OCH_3$ ⟶ $C_6H_5OH + H_2C{=}O$	Codeine
Oxidative deamination	$(CH_2)_2CHNH_2$ ⟶ $(CH_3)_2C{=}O + NH_3$	Amphetamine
S-oxidation	CH_3SCH_3 ⟶ $CH_3S{=}O$	Chlopromazine
Reductive dehalogenation	$C_6H_5CH_2Br$ ⟶ $C_6H_5CH_3$	Halothane

Table 1. Major types of reactions catalyzed by cytochromes P450

The first cytochrome P450 enzyme to be crystallized was P450 camphor 5-exohydroxylase ($P450_{cam}$) from the soil bacterium Pseudomonas putida. This enzyme catalyzes the regiospecific and stereospecific hydroxylation of D-camphor by using molecular oxygen and two electrons from NADH (Figure 4).

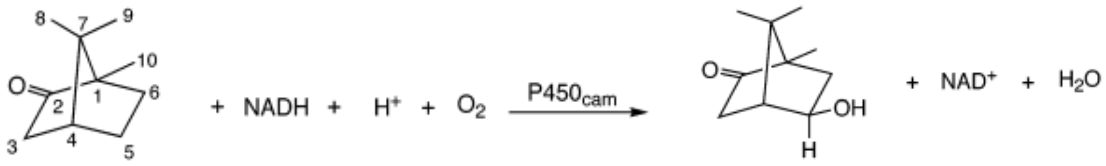

Figure 4. Hydroxylation of D-camphor by $P450_{cam}$

$P450_{cam}$, was intensively studied, and all the investigations carried out on its structures and functions helped elucidate the catalytic cycle of cytochrome P450 for the hydroxylation of the C-H bond. In particular, as all P450 enzymes, it presents a sulfur atom of a proximal cysteine residue as the axial ligand to the heme iron (Figure 5 a). Moreover, regarding the catalytic pathway, a generally accepted mechanism has been supposed and it involves the initial hydrogen atom abstraction from a C-H bond of the substrate, followed by the recombination of the resultant radical species to form the hydroxylated product (Figure 5 b). Interestingly, during HAA reaction, the proton transfers from carbon to the oxygen of compound I ($Fe^{IV}{=}O$), but the electron is transferred to the porphyrin radical cation.

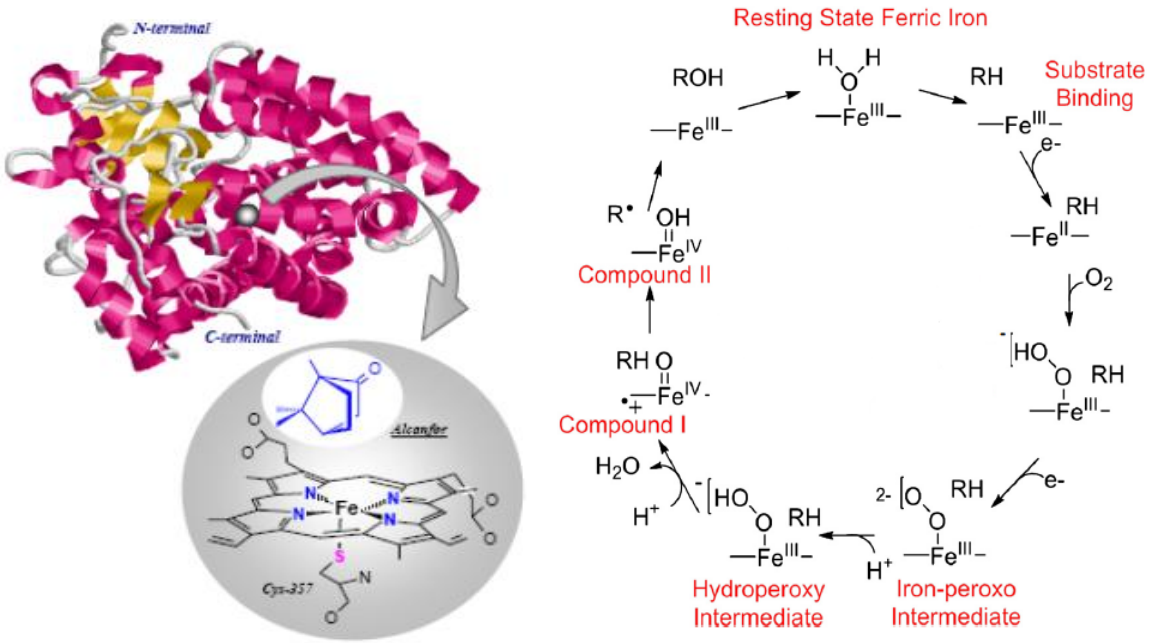

(a) **(b)**

Figure 5. (a) Structure of $P450_{cam}$; **(b)** catalytic cycle of cytochrome P450 for the hydroxylation of a C-H bond

1.3 Biomimetic catalysts and model complexes

Enzymatic oxidation reactions have emerged on an industrial scale. An example is the oxidation of D-glucose to D-gluconolactone using the enzyme glucose oxidase (GO) (Figure 6 a), and the production of hydroxy amino acids using L-isoleucine dioxygenase (IDO) (Figure 6 b). D-gluconolactone has been used in the food and wine industry, whereas the hydroxy amino acids are promising compounds for drugs and functional foods due to antidiabetes activity.[1]

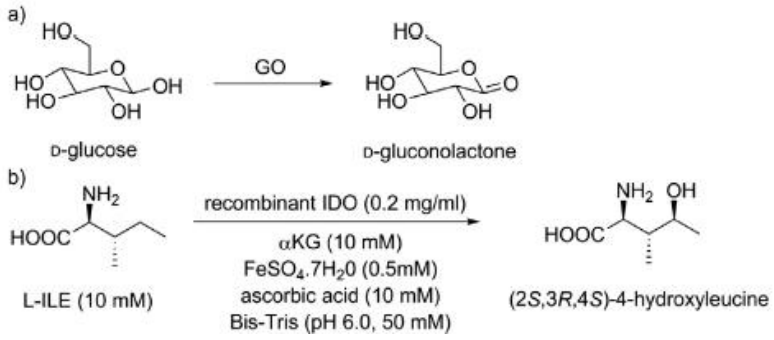

Figure 6. (a) Oxidation of D-glucose to D-gluconolactone **(b)** Production of hydroxyl amino acids

Nonetheless, the application of natural enzymes in industrial scale processes is still hampered by different factors. The main limitations are enzyme stability and productivity. For these reasons the synthesis of bioinspired complexes has gained great relevance. Moreover, mechanistic studies of biomimetic catalysts can improve the knowledge about metalloenzyme structure and function and provide important insights into biological pathways. Among the bioinspired complexes, mononuclear metal-oxos are the most widely studied intermediates. Iron-oxo species, both in synthetic and enzymatic systems, have been observed for the first time in the 1980s.[12-14] By contrast, the isolation and spectroscopic characterization of a mononuclear non-heme iron(IV)−oxo species $[(TMC)Fe^{IV}(O)(CH_3CN)]^{2+}$ (TMC = 1,4,8,11-tetramethyl-1,4,8,11-tetraazacyclotetradec-ene) occurred more recently, in 2003 (Figure 7).[9]

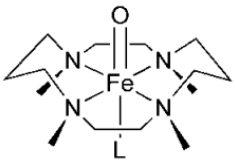

Figure 7. Structure of $[(TMC)Fe^{IV}(O)(L)]^{2+}$ ($L=CH_3CN$)[8]

This complex was prepared using iodosylbenzene (PhIO) as an oxidant in CH_3CN at − 40 °C. Other oxidants, such as hydroperoxides (e.g., H_2O_2 and alkyl hydroperoxides), peracids, NaOX (X = Cl or Br), O_3, R_3NO, and N_2O, were also used as single-oxygen atom donors to generate iron(IV)-oxo complexes at low and room temperatures. $[(TMC)Fe^{IV}(O)(CH_3CN)]^{2+}$ showed to be a competent OAT agent by reaction with PPh_3, and its ability of performing hydrogen atom abstraction (HAA) was confirmed by reaction with phenol. Interestingly, the reactivity of the iron(IV)-oxo complex both in HAA and OAT was found to vary significantly depending on the axial ligand.

1.3.1 Model complexes based on late transition metals

After $[(TMC)Fe^{IV}(O)(CH_3CN)]^{2+}$, many other non-heme metal-oxo complexes have been synthesized and characterized by various spectroscopic techniques as well as by X-ray crystallography. Most of these complexes showed to be capable in the oxidation of numerous substrates for HAA and OAT reactions, including inert alkanes.[15-17] Moreover, it was investigated how their reactivity is modulated by ligand effects, the presence of Lewis acids, and other conditions. The general procedure for the synthesis of non-heme metal-oxo complexes (Figure 8) involves the reaction of the reduced metal complexes $[LM^{n+}]$ with an oxo transfer agent such as PhIO, N_2O or a peracid; dioxygen in the presence of H atom donors; water in the presence of an oxidant; and hydrogen peroxide with a base; dioxygen in the presence of H atom donors or Sc^{3+} ion and a reducing agent.

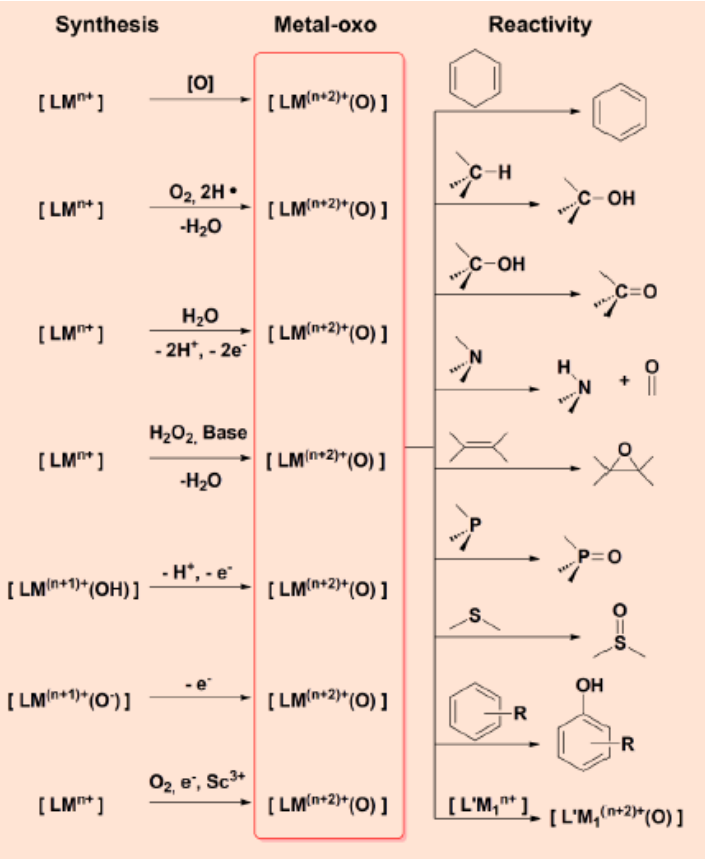

Figure 8. Synthesis of biomimetic high-valent metal-oxo complexes and their reactivity with different substrates

Over the last years, much attention has been paid on oxo complexes based on late transition metals, particularly Co, Ni and Cu. They are expected to be powerful oxidant, perhaps even more reactive than the related iron-oxo complexes. Computational studies[18] investigated the reactivity of a series of Fe, Co and Ni oxo complexes supported by bidentate ligands, and predicted them to be capable of activating methane. From the results obtained, emerged that later transition metals are more reactive. Particularly, the most promising C-H activation catalysts were found to be Ni^{III}=O complexes featured by a fluorinated β-diketiminate ligand and a calculated activation barriers as low as 8.1 kcal/mol. Overall, oxo complexes of the late transition metals (Co, Ni and Cu) have been considered potential reactive intermediates in various chemical and biological oxidation reactions. Nonetheless, no ‘’pure’’ oxo complexes of these metals has been isolated so far. Many studies have been carried out for establishing structural motifs capable of stabilizing the M-O group. Regarding naturally occurring enzymes, structure-function investigation on metallo-proteins suggest that intramolecular hydrogen bonds can

regulate the properties of the oxo-metal complex. Particularly, such interactions occur between the oxo moiteis and a H-bond donor(s) located within the active site. In this regard, Borovik's group employed a polidentate ligand that binds metal ions and promotes intramolecular H-bonds to M-O(H) units: $[Fe^{III}(O)(H_3buea)]^{2-}$(buea = tris[(N'-tertbutylureaylato)-Nethyl)]aminato) (**2**, Figure 9).[19]

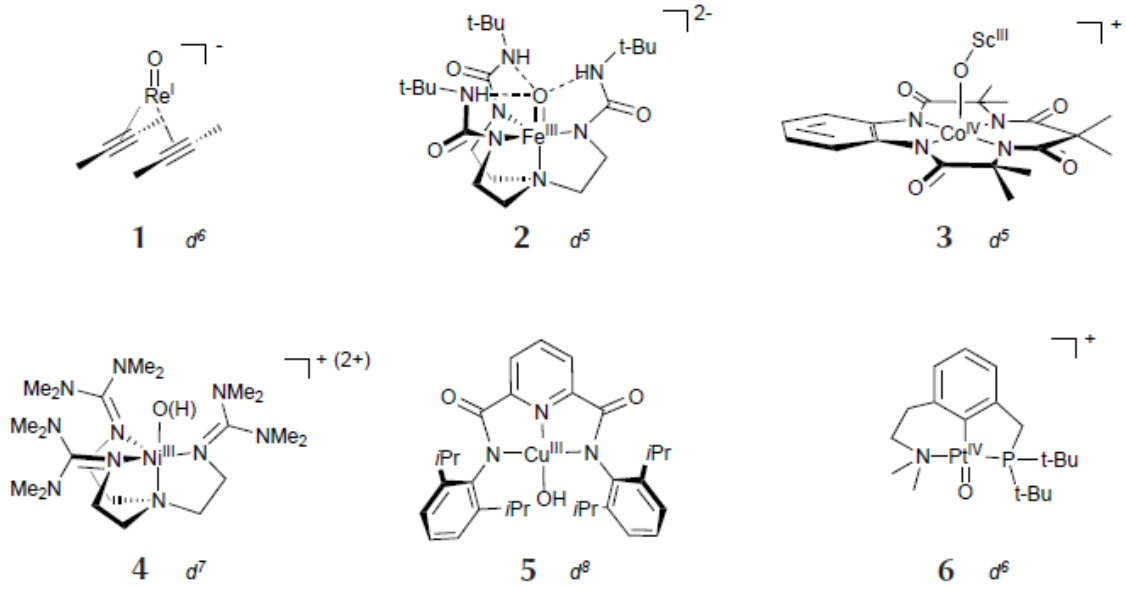

Figure 9. Examples of late-transition metal oxo and metal-oxygen adducts

In other cases, strongly π-accepting ligands can bind the metal centre in order to delocalize the *d* electron density: $[Re^{I}(O)(alkyne)_2]$ (**1**, Figure 9).[20] Moreover, also the binding of a Lewis acid to the metal can increase the electrophilicity of the oxygen atom,[21] [(TAML)Co^{IV}-O-Sc] (**3**, TAML = tetraamidomacrocyclic ligand) or protonation in the nickel and copper complexes[22,23] (**4**, **5**, Figure 9). Because of the greater stabilization, these species have shown to be less reactive compared to the predicted pure oxo complex. Milstein's group isolated a late transition metal-oxo platinum(IV)=O complex (**6**, Figure 9).[24] Such complex involved a meridional, tridentate ligand framework and was obtained by reacting the square-planar Pt^{II} precursor with dimethyldioxirane. It was capable of activating water yielding a dihydroxo complex, but not reactive towards HAA and OAT substrates. Such behavior could be due to the great metal-ligand bond strength and the stability of the high oxidation states for third-row metals, compared to the first row.

1.3.2 Nickel-containing enzymes

Only a few nickel-containing enzymes are known, but they play an important role in the metabolic activity of different microorganisms. Biological processes mediated by these enzymes include: urea hydrolysis (Urease), reversible hydrogen oxidation ([NiFe]-hydrogenase), interconversion of carbon monoxide and carbon dioxide (Carbon monoxide dehydrogenase CODH), convertion of CO_2 and a methyl group to acetyl-CoA (acetyl-CoA synthetase (ACS) in concert with CODH), methane generation (Methyl-coenzyme M reductase MCR), and dismutation of superoxide (Superoxide dismutase Ni-SOD).[25] Consistent with their disparate functions, these enzymes present different metallocenter structures which vary according to the coordination geometry, the number and nature of the metal, the presence of additional components (Figure 10).

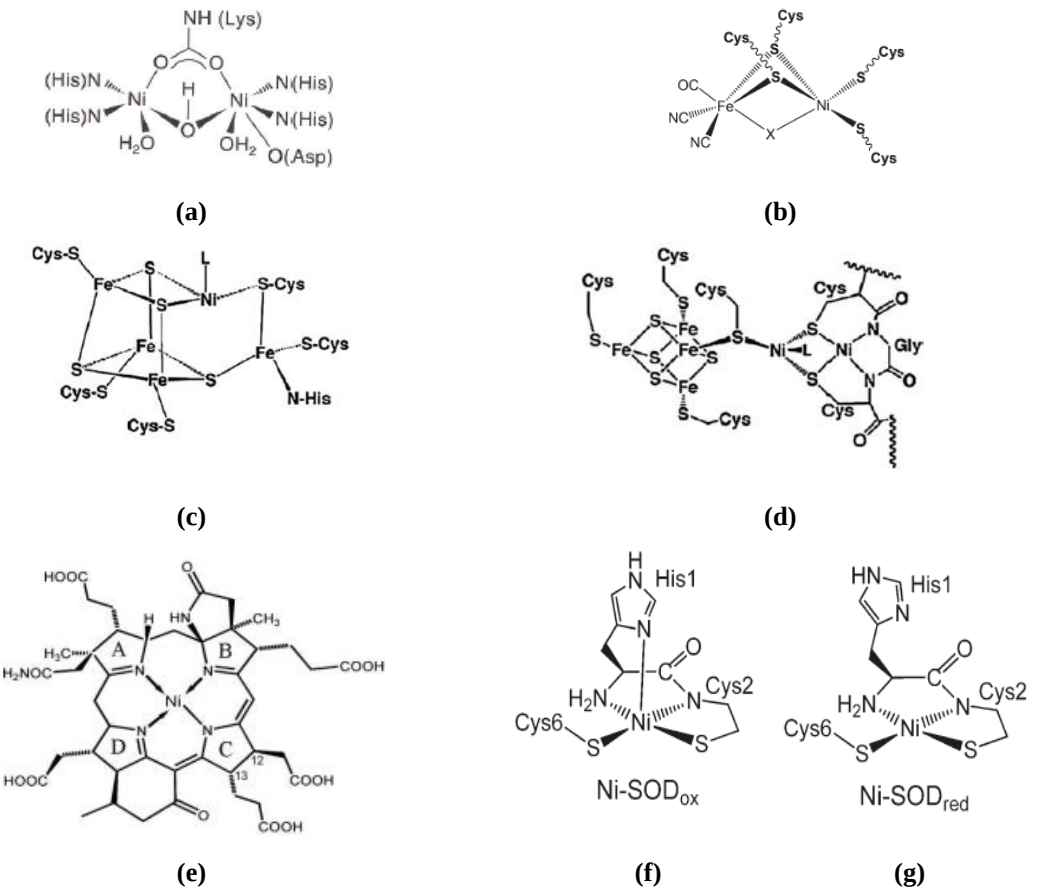

(a) **(b)** **(c)** **(d)** **(e)** **(f)** **(g)**

Figure 10. (a) Structure of the dinuclear nickel active site of urease; **(b)** structure of [NiFe]-hydrogenases; **(c)** structure of synthase carbon monoxide dehydrogenase (CODH); **(d)** acetyl-CoA Synthase (ACS); **(e)** F_{430} cofactor of methyl-coenzyme M reductase (MCR); **(f)** Superoxide dismutase Ni-SOD oxidated form; **(g)** Superoxide dismutase Ni-SOD reduced form;

Enzyme	Reaction catalyzed
Urease	$Urea + H_2O \longrightarrow 2\ NH_3 + H_2CO_3$
Hydrogenase	$2\ H^+ + 2\ e^- \rightleftharpoons H_2$
CO Dehydrogenase	$CO + H_2O \rightleftharpoons 2\ H^+ + CO_2 + 2\ e^-$
Acetyl-CoA Synthase	$CH_3\text{-}CFeSP + CoASH + CO \longrightarrow CH_3\text{-}CO\text{-}SCoA + CFeSP$
Methyl-CoM Reductase	$Methyl\text{-}SCoM + CoBSH \longrightarrow CH_4 + CoBS\text{-}SCoM$
Superoxide Dismutase	$2O_2^- + 2H^+ \longrightarrow H_2O_2 + O_2$

Table 2. Reactions mediated by nickel enzymes

1.3.2.1 Urease

Urease was the first nickel enzyme to be isolated and it plays a central role in the nitrogen metabolism of many plants, fungi, and bacteria. It catalyses the hydrolysis of urea to ammonia and carbamate, which spontaneously decomposes to give carbonic acid and a second molecule of ammonia (Figure 11).[26] The enzyme involves a dinuclear Ni-active site in which the two metals are bridged by a carbamylated lysine residue (Figure 10 a). One Ni^{II} (so-colled Ni-1) is five-coordinated while the other (Ni-2) is described as ‘’pseudotetraedral’’. During the reaction, Ni-1, acting as a Lewis acid, is thought to coordinate and polarize the carbonyl oxygen of urea, and Ni-2 is supposed to activate a bonded solvent molecule that performs the hydrolysis reaction releasing ammonia.

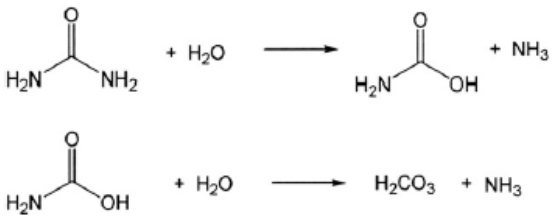

Figure 11. Hydrolysis of Urea catalyzed by Urease enzyme

1.3.2.2 [NiFe]-hydrogenases

Hydrogenases play a key role in the energy metabolism of various microorganisms. They catalyze the reversible two-electron oxidation of molecular hydrogen.[27] Hydrogenases are divided into three classes according to the metal centre: [NiFe]-hydrogenases, [FeFe]-hydrogenases [Fe]-hydrogenases. In particular, [NiFe]-hydrogenases contain three iron–sulfur clusters and a bimetallic Ni/Fe active site (Figure 10 b). Nickel and iron atom are bridged by two thiolates of cysteines from the protein backbone. Moreover, three diatomic non-protein ligands are bound to the Fe (two CN^- and one CO) and two other cysteine thiolates coordinate the nickel in a terminal fashion. A third bridging ligand between these metals is temporarily present depending on the respective apparent oxidation state.[28]

1.3.2.3 Synthase carbon monoxide dehydrogenase (CODH) and Acetyl-CoA synthetase (ACS)

Numerous methanogenic and acetogenic bacteria contain Synthase carbon monoxide dehydrogenase (CODH) which catalyzes the oxidation of carbon monoxide to carbon dioxide in a reversible, two-electron process. Moreover together with Acetyl-CoA Synthase (ACS), it forms the bifunctional enzyme ACS/CODH which catalyze the reversibile formation of Acetyl-CoA in combination with CoA itself and a methyl source. CODH is a [3Fe-4S] cluster bridged to a heterodinuclear [NiFe] site (Figure 10 c) , whereas ACS consists of a [4Fe-4S] cubane unit linked via a bridging cysteine residue to a proximal nickel ion which, in turn, is coordinated (by two cysteine bridges) to a square-planar distal nickel centre (Figure 10 d).

1.3.2.4 Methyl-coenzyme M reductase MCR

Methyl-coenzyme M reductase (MCR) is the key enzyme of methane formation in methanogenic bacteria.[29] This enzyme converts 2-methylthioethanesulfonate (methyl-SCoM) and N-(7-mercaptoheptanoyl)threonine 3-O-phosphate (CoBSH) into methane

and the heterodisulfide CoB-S-S-CoM (Figure 12). Regarding the structure of the enzyme, MCR has two active sites each occupied by the nickel containing F_{430} cofactor. Such cofactor features a highly hydrogenated porphyn system with anellated lactam and cyclohexanone rings (Figure 10 e).

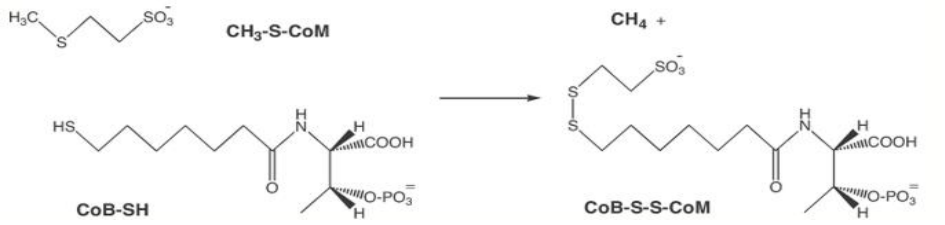

Figure 12. Methane formation in methanogenic bacteria

1.3.2.5 Nickel superoxide dismutase (Ni-SOD)

Superoxide dismutases (SODs) are a family of metalloenzymes that protect organisms from the superoxide anion radical ($O_2^{\bullet -}$): a cytotoxic byproduct of the aerobic methabolism. These enzymes are capable to catalyze the disproportionation of superoxide anion radical to peroxide and molecular oxygen through alternate oxidation and reduction of the catalytic metal centres. Superoxide dismutases employing metal ions Fe, Cu/Zn and Mn, have been extensively characterized. By contrast not much is known about Ni-containing SOD and its reaction mechanism. Regarding the structure of the enzyme, Ni-SOD is made up of six identical subunits and which contains a single nickel active site. The reduced enzyme has a square-planar geometry where the nickel metal centre is coordinated to a primary amine-N of His-1, carboxamido-N from Cys2 and two thiolato-S donor atoms from Cys2 and Cys6 (Figure 10 g). The oxidation causes a change in the coordination geometry. Indeed, Ni^{III} binds the N-terminal histidine group in the axial position and result in the formation of a square-pyramidal metal centre (Figure 10 f). Moreover, the presence of the two coordinated cysteine thiolates, is supposed to be responsible for the modulation of the Ni^{III}/Ni^{II} redox couple to a value suitable for physiological function.

1.3.3 Nickel model complexes

Nickel exists in oxidation states ranging from 0 to IV, and all (except IV states) have been observed in biology. The II oxidation state is the most stable, nonetheless most nickel-based enzymes appear to access either the II/I and/or the III/II redox couples.[30] Thanks to the striking flexibility of these enzymes in redox chemistry, many model complexes have been developed in order to mimic that catalytic activity. During the 80s and 90s, several catalysts for olefine epoxidation were designed based on different N, O, P-ligated Ni^{II} salts. Kochi and Burrow studied the efficiency of nickel (II) complexes bearing macrocyclic ligands in the oxidation of several alkenes. They suggested Ni^{IV}=O as oxygen atom transfer agent, but the species was never observed. Moreover, competitive ligand and solvent oxidations, could indicate the ability of these complexes to promote hydrocarbon oxidation. Recently, Palanandaviar's group obtained several Ni^{II} complexes supported by pentadentade ligands capable of alkane hydroxylation.

3-chloroperoxybenzoic acid (m-CPBA) was employed as oxidant and the substrates oxidized were cyclohexane, adamantane and cumene. The formation of both Ni^{III}=O and Ni^{IV}=O intermediates have been predicted by computational studies. Furthermore, some nickel-contaning complexes have been demonstrated to be effective catalysts for water oxidation. To date, very few high-valent nickel-oxygen adducts ($Ni^{III/IV}$–OX) have been isolated and characterized.[31] For example, Latos–Grazynski[32] reacted a Ni^{III}-porphyrinoid bromide with sodium hydroxide to afford a new species claimed to be Ni^{III}-OH. However, the complex was only characterized by EPR and its reactivity was not investigated. Ray's group treated $[Ni^{II}(TMG_3tren)(OTf)](OTf)$ (TMG_3tren = (tris[2-(Ntetramethylguanidyl)ethyl]amine, OTf = trifluoromethanesulfonate) with mCPBA at low temperature and reported the formation of two EPR-active species identified as nickel-hydroxo complexes (Ni^{III}-OH).[22] Nonetheless, the low yield (15%) and the presence of two Ni^{III} species in the reaction mixture hampered further characterization. Liaw and Chiu synthesized Ni^{III}–OMe and Ni^{III} –OPh complexes but no reactivity study were performed. Interestingly, some high-valent bimetallic bis(μ-oxo) complexes, ($[Ni^{III}(\mu\text{-}O)Ni^{III}]$[33-38], and $[Ni^{III}(\mu\text{-}O)Cu^{III}]$[39]) have been obtained and found to be competent HAA agents. Lately, high-valent terminal nickel-oxygen species, and particularly the oxo complexes, have started to gain attention. Indeed, their isolation and characterization could help us understand further the reactivity properties of late

transition metal oxidants. Moreover, they would greatly contribute to improve the design of new and effective oxidation catalysts

1.3.4 Nickel complexes of the pyN_2^{R2} ligands

Depending on the nature of the ligand, the Ni(II) ion (d^8) can form tetrahedral, octahedral or square planar complexes. In general, the square planar geometry is promoted by strong field ligands, whereas weak field ligands yield tetrahedral and octahedral complexes depending on the steric hindrance. Particularly, the square planar geometry is favored by strong field multidentate ligands such as tridententate pincer ligands. These pincer ligands are a type of chelating agents that bind tightly, to three adjacent coplanar sites, the metal centre in a meridional configuration.

Interestingly, they feature a great conformational rigidity that makes them extremely resistant to several common degradation pathways.

Thanks to these benefits they are frequently employed in catalysis. Tolman employed the pincer ligand N,N'-bis(2,6-diisopropylphenyl)-2,6 pyridinedicarboxamidate $[pyN_2^{R2}]^{2-}$ (R = iPr) (Figure 13 a) for the synthesis of his high-valent copper-hydroxo complex **(**Cu^{III}-OH) (see **5**, Figure 9).

We also identified this class of ligands, as excellent for investigating the behavior of terminal high-valent nickel-oxygen adducts. These ligands bear, as donor sites, three nitrogen atoms, which are able to efficiently stabilize high oxidation states of the metal centre because of their strong σ-donating ability. Moreover they are exceedingly resistant to hydrolytic and oxidative degradation. Still, methyl groups can be introduced in the ortho position of the N-phenyl groups instead of the iso-propyl groups affording $[pyN_2^{Me2}]^{2-}$ (Figure 13 b). The protonated form of the ligand $[pyN_2^{iPr2}]^{2-}$ and $[pyN_2^{Me2}]^{2-}$ is depicted in figure 13.

(a) **(b)**

Figure 13. (a) Pincer ligand $H_2pyN_2^{iPr2}$; **(b)** pincer ligand $H_2pyN_2^{Me2}$

During the synthesis of the complexes, a strong base ([Et_4N][OH] or NaH) deprotonates the ligand making it dianionic. In this form, the ligand coordinates the metal ion by the three nitrogen donor atoms. Finally, upon the coordination of the metal to the ligand, the fourth coordination site can be occupied by a neutral or anionic monodentate group.
In this work, anionic Ni(II) complexes (Figure 14 a) were more attractive compared to the neutral one (Figure 14 b). Indeed, thanks to the excess of negative charge, the anionic Ni(II) species were more easily oxidizable to the Ni(III) complexes.

$[Ni^{II}(pyN_2^{R2})(X)]^-$ (X = anionic ligand) $[Ni^{II}(pyN_2^{R2})(L)]$ (L = neutral ligand)

(a) **(b)**

Figure 14. General structure of **(a)** Anionic Ni(II) complexes and **(b)** neutral Ni(II) complexes

1.4 Aims of this work

The aim of this project was to investigate the reactivity of high-valent Ni(III) complexes in hydrogen atom abstraction (HAA) and oxygen atom transfer (OAT) reactions. In particular, this work is divided into three parts:

1. synthesis of the Ni(II) complexes;
2. oxidation of the Ni(II) complexes to Ni(III) species;

3. reaction of the Ni(III) species with different organic substrates in order to probe their HAA and OAT reactivity.

During the first part of the project, we synthesized several Ni(II) complexes, of the type $[Ni^{II}(pyN_2^{R2})(L)]$ and $[Ni^{II}(pyN_2^{R2})(X)]^-$, which vary according on the monodentate group in the fourth coordination position site. $H_2pyN_2^{R2}$ (R= CH_3, iPr) were selected as ideal pincer ligand for the stabilization of the high oxidation states of the metal. In particular, we decided to focus our work exclusively on nickel species featured by $[pyN_2^{Me2}]^{2-}$. Indeed, $H_2pyN_2^{iPr2}$ ligand was employed just once in order to explore alternative synthetic pathways for the synthesis of our complexes.

Since, the Ni(III) species have shown to be very unstable, their synthesis (part 2 of the project), and their reactions with organic substrates (part 3 of the project) were carried out at low temperature (- 40°C or -80 °C). Moreover, in order to improve the yield of the Ni(III) species many different experimental conditions were explored during the oxidation of the Ni(II) species.

The OAT and HAA reactions were performed by adding triphenylphosphine (PPh_3) (at -80 °C) and 2,6-di-tert-butylphenol (2,6-DTBP) (at -40 °C) to the in situ generated Ni(III) complexes, respectively. These substrates are the most employed in literature for this purpose, but in order to gain further insight into the hydrogen atom abstraction reaction also several phenols, which differ according to the steric hindrance, were used during this work.

Ni(II) species were characterized by ^{1}H NMR, IR, MS, Uv-vis spectroscopy, whereas Ni(III) complexes, were identified by EPR and Uv-vis spectroscopy, because unstable at room temperature. Conversely, the organic products obtained from HAA and OAT reactions, were detected by ^{1}H NMR and MS analyses. The reactions were monitored by UV-vis spectroscopy examining the change in absorbance of the main electronic features. Overall, the preparation and isolation of high-valent nickel species will help to provide mechanistic insights into oxidation catalysis and improve the knowledge about the high-valent iron species equivalents.

2. Results and discussion

2.1 Synthesis of Ni(II) complexes

2.1.1 Synthesis of $[Et_4N][Ni^{II}(pyN_2^{Me2})(OH)]$ (8)

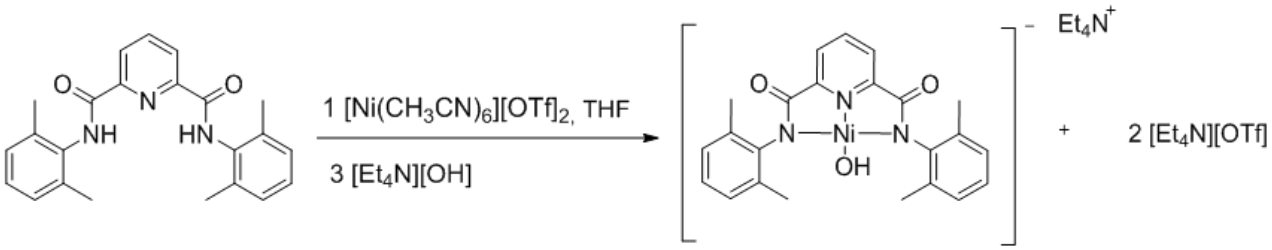

Figure 15. Synthesis of $[Et_4N][Ni^{II}(pyN_2^{Me2})(OH)]$ (**8**)

The nickel complex $[Ni^{II}(pyN_2^{Me2})(OH)]^-$ (**8**) was synthesized by deprotonating $H_2pyN_2^{Me2}$ (dissolved in THF) with 3 equivalents of $[Et_4N][OH]$, and reacting the resulting solution with $[Ni(CH_3CN)_6][OTf]_2$ (Figure 15). The reaction mixture was stirred for 12 h to afford a deep red solution and some sticky precipitate. The day after, work up and crystallization from DMF and diethyl ether, yielded a red crystalline **8** (60%). In order to improve the removal of tetraethylammonium triflate, washing with toluene as well as a crystallization from methanol and THF were performed. Nonetheless, both processes were found to be less efficient compared to the crystallization from DMF and diethyl ether.

The nature of the complex was confirmed by UV-vis, ^1H NMR and ATR-FTIR spectroscopies. The Uv-vis spectrum of **8** showed a strong absorption at $\lambda_1 = 411$ nm and a shoulder at $\lambda_2 = 483$ nm. As expected the IR spectrum displayed the presence of O-H stretching band at ca. 3600 cm^{-1}. This result was consistent with ^1H NMR spectrum where the hydroxyl group was confirmed by the singlet peak at – 4,89 ppm. That upfield –OH resonance (– 4,89 ppm) can be attributed to its position in the shielding cone of the two side aryl groups.

The reaction is likely to proceed via formation of the neutral $[Ni^{II}(pyN_2^{Me2})(CH_3CN)]$ intermediate followed by substitution of CH_3CN with OH^-. Thus two equivalents of

[Et_4N][OH] are required for the deprotonation of $H_2pyN_2^{Me2}$ whereas the third equivalent provides the OH^- ligand. This procedure yielded compound **8** contaminated by two equivalents of tetraethylammonium triflate. Since it was not possible to separate the two salts, all the later uses of the mixture involved compound **8** along with the two equivalents of by-product [Et4N][OTf].

2.1.2 Synthesis of [Et_4N][$Ni^{II}(pyN_2^{Me2})(OCO_2H)$] (10)

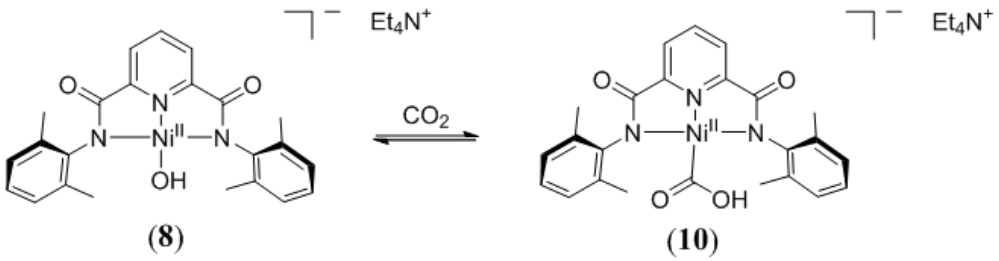

(**8**) (**10**)

Figure 16. Synthesis of [Et_4N][$Ni^{II}(pyN_2^{Me2})(OCO_2H)$] (**10**)

The bicarbonate derivative **10** is obtained by reacting **8** with CO_2. Indeed **8** is very sensitive to CO_2 and **10** is partially formed even by exposing an acetone solution of **8** to atmospheric CO_2.

Improved yields are obtained after bubbling CO_2 through a solution of **8** for 15 minutes (Figure 16). Diffusion of diethyl ether into the reaction mixture yielded an orange-red crystalline solid (yield 85 %). As expected, the ^{1}H NMR spectrum of **10** differs from that of **8** by the absence of the OH signal. Moreover it was characterized by Uv-vis spectroscopy and it showed a strong absorption at $\lambda_1 = 380$ nm and a shoulder at $\lambda_2 = 475$ nm (see section 2.2 figure 25).

2.1.3 Synthesis of [Et_4N][$Ni^{II}(pyN_2^{iPr2})(OH)$] (11)

In order to obtain a hydroxo complex analogous to 8 but without impurities of [Et_4N][OTf]$_2$, we set out to synthesize a Ni(II) complex (complex **11**) with a different ligand: $H_2pyN_2^{iPr2}$. Using this isopropyl-substituted ligand offers two important

advantages compared the methyl analogue. First, it provides a higher degree of steric protection to the reactive oxygen moiety; second, its complexes are more soluble in organic solvents, allowing a better separation from side products.

Regarding **11**, different synthetic pathways were investigated in order to find the best reaction conditions and increase the yield. All the procedures employed followed the same reaction scheme featuring two different steps. The first step consisted in the synthesis of the neutral complex $[Ni^{II}(pyN_2^{iPr_2})(CH_3CN)]$ (**9**) which contains a labile and easily replaceable acetonitrile ligand in the fourth coordination position. The second step consisted in a ligand exchange reaction by adding 1 equivalent of $[Et_4N][OH]$. The first synthetic pathways was performed by deprotonating $H_2pyN_2^{iPr2}$ dissolved THF with NaH, and reacting the resulting solution of $Na_2pyN_2^{iPr2}$ with $[Ni(CH_3CN)_6][OTf]_2$ (Figure 17). This step led to the formation of the neutral complex $[Ni^{II}(pyN_2^{iPr2})(CH_3CN)]$ (**9**) where the acetonitrile group binding the metal centre is provided by the nickel salt. Finally, during the second step, the addition of 1 equivalent of $[Et_4N][OH]$ afforded **11** in 49 % yield.

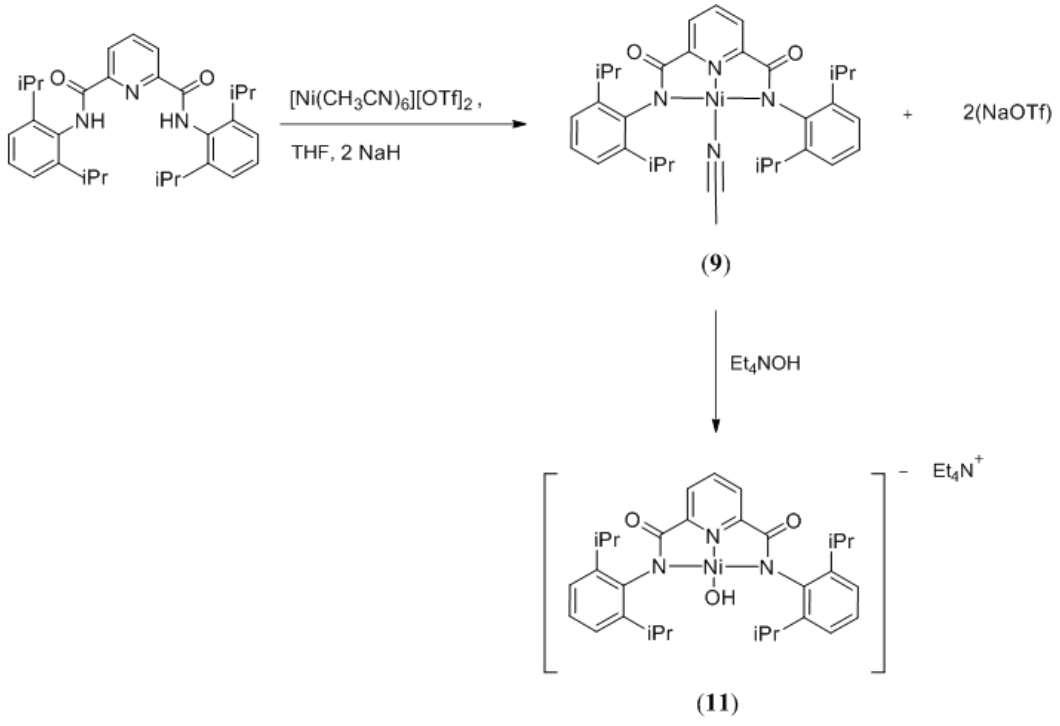

Figure 17. Synthesis of **11** with $[Ni(CH_3CN)_6][OTf]_2$.

In order to find an alternative to $[Ni(CH_3CN)_6][OTf]_2$, which is highly hygroscopic, difficult to handle and expensive, we decided to perform the same reaction, first with $Ni(OAc)_2 \cdot 4\ H_2O$ and then with $Ni(OTs)_2$ (Figure 18). Since these two nickel salts don't bear an acetonitrile group, CH_3CN was added as reagent, along with THF as solvent, in order to form complex $[Ni^{II}(pyN_2^{iPr_2})(CH_3CN)]$ (**9**).

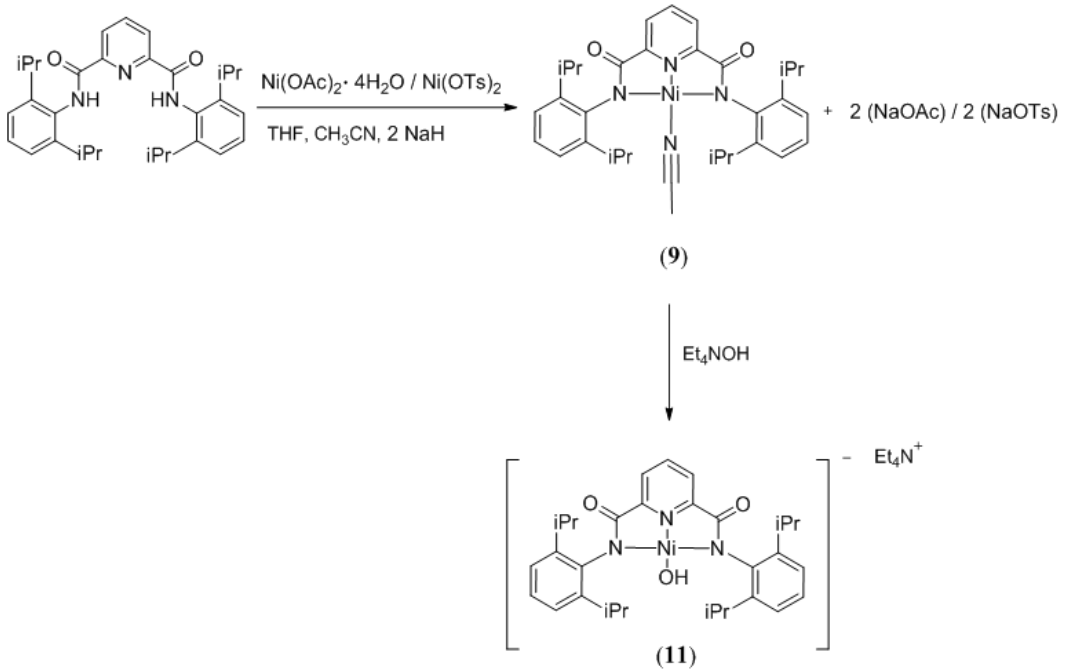

Figure 18. Synthesis of **11** with $Ni(OAc)_2 \cdot 4\ H_2O$ or $Ni(OTs)_2$.

Overall, the procedure carried out with $Ni(OTs)_2$ allowed to obtain the product in a 24 % yield, whereas the reaction with $Ni(OAc)_2 \cdot 4\ H_2O$, yielded the product in a trace amount. Likely, the low yields obtained with both nickel salts were due to their limited solubility in THF. Altogether, these results let us to conclude that $[Ni(CH_3CN)_6][OTf]_2$ gave the best results in term of yield.

2.1.4 Synthesis of [$Ni^{II}(pyN_2^{Me2})(CH_3CN)$] (13)

After the synthesis of **9**, we decided to focus our attention on another nickel complex: [$Ni^{II}(pyN_2^{Me2})(CH_3CN)$] (**13**). The structure of **13** is similar to that of **9**; it shows the same acetonitrile group in the fourth coordination site but another tridentate pincer ligand ($H_2N_2py^{Me2}$) binding the metal centre. The synthesis of **13** was set out in order to use it as starting material for the synthesis of other Nickel(II) complexes. Indeed, since the acetonitrile group (as in complex **11**) is labile and easily replaceable, three different nickel complexes were then obtained from **13** by ligand exchange: [Et_4N][$Ni^{II}(pyN_2^{Me2})(Cl)$] (**14**), [Et_4N][$Ni^{II}(pyN_2^{Me2})(OC(O)CH_3)$] (**15**) and [$Et_4N$][$Ni^{II}(pyN_2^{Me2})(OC(O)H)$] (**25**) (see paragraph 2.1.5).

Regarding the synthesis of **13**, three different procedures were carried out. The first was performed by using $Ni(OTs)_2$ and following the same procedure employed for **9** where CH_3CN was added as reagent and THF as solvent. After, since $H_2pyN_2^{Me2}$ was found to be less soluble in THF compared to $H_2pyN_2^{iPr2}$, an alternative procedure was carried out by using exclusively acetonitrile, which played the role of solvent and reagent at same time. This alternative procedure was performed twice, first with $Ni(OTs)_2$ and then with $[Ni(CH_3CN)_6][OTf]_2$ as starting materials.

The first procedure reacting $Ni(OTs)_2$ with $H_2pyN_2^{Me2}$ and NaH, using THF as solvent and acetonitrile as reagent, yielded a sodium salt of the nickel complex: [Na][$Ni^{II}(pyN_2^{Me2})(OTs)$] (**17**) (Figure 19).

The formulation of this compound was based on the ^1H NMR spectrum of the final mixture because of the absence of the expected resonance of the CH_3CN group (a singlet peak at $\delta = 1.29$ ppm). Instead, a singlet at $\delta = 2.35$ ppm and two dublets at 7.21 and 7.68 ppm are indicative of the presence of the TsO^- group. Another evidence supporting our hypothesis was the higher solubility of the final product in methanol compared to that in chloroform. Indeed, the expected product [$Ni^{II}(pyN_2^{Me2})(CH_3CN)$] (**13**) should have been neutral and therefore more soluble in $CHCl_3$.

All the data collected, led us to suppose that most likely OTs^- group should have replaced the acetonitrile ligand in the fourth coordination position promoting the formation of Na[$Ni^{II}(pyN_2^{Me2})(OTs)$] (**17**) instead of that of [$Ni^{II}(pyN_2^{Me2})(CH_3CN)$] (**13**).

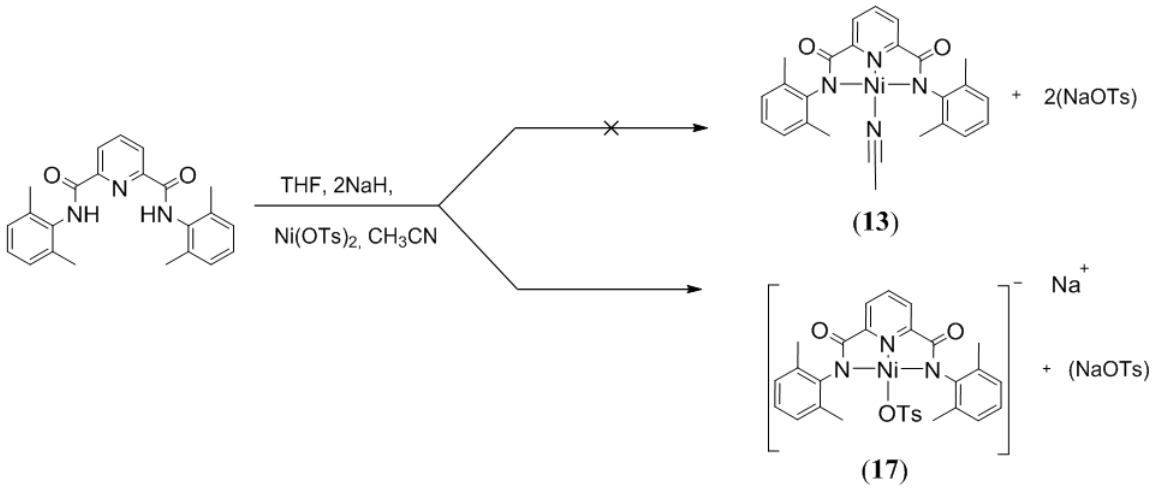

Figure 19. Synthesis of **13** with $Ni(OTs)_2$ and THF as solvent and acetonitrile as reagent

Afterwards, no improvements were obtained by performing the alternative procedure with $Ni(OTs)_2$ exclusively in acetonitrile (Figure 20). Indeed, also under these conditions ^1H NMR analyses of the final mixture confirmed the formation of the ionic compound $[Na][Ni^{II}(pyN_2^{Me2})(OTs)]$ (**17**).

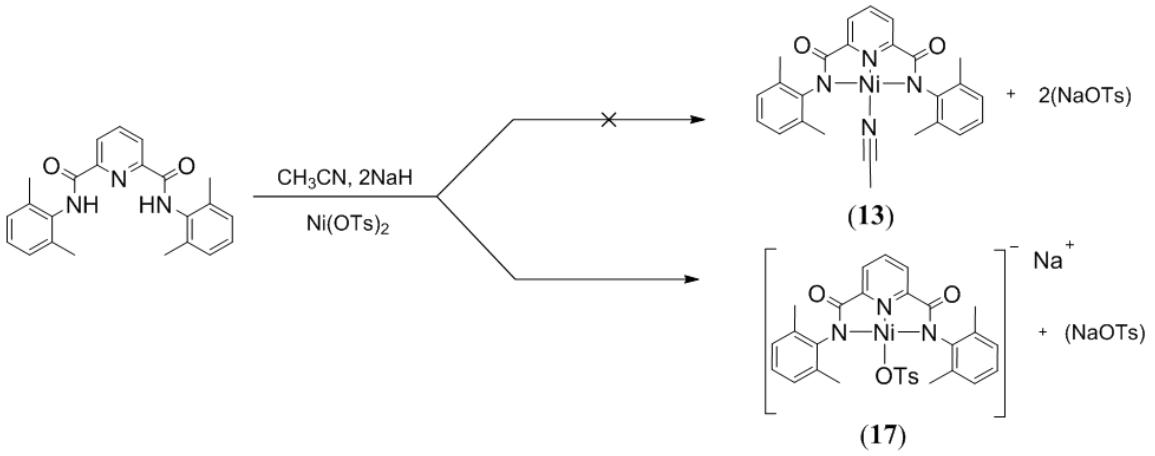

Figure 20. Synthesis of **13** with $Ni(OTs)_2$ and acetonitrile

Finally, the best reaction conditions for the synthesis of **13** were found employing $[Ni(CH_3CN)_6][OTf]_2$ in neat acetonitrile in the presence of $H_2pyN_2^{Me2}$ and NaH (Figure 21). Indeed, this last procedure allowed us to obtain the expected neutral complex **13** in satisfactory yields.

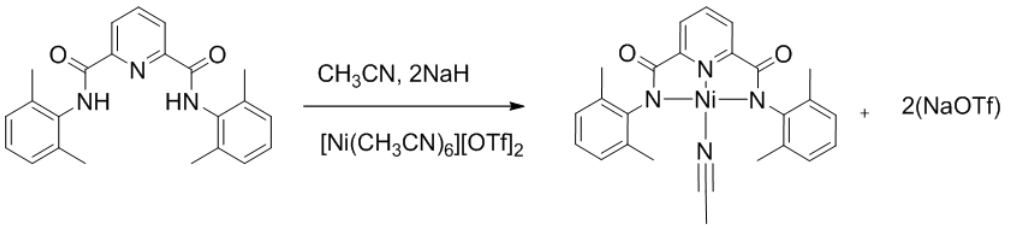

(**13**)

Figure 21. Synthesis of **13** with $[Ni(CH_3CN)_6][OTf]_2$ and acetonitrile

As for the synthesis of **11**, $[Ni(CH_3CN)_6][OTf]_2$ showed to be the most reactive nickel salt allowing us to isolate the expected product. Compound **13** was characterized by H^1 NMR, IR, MS and UV-vis spectroscopy. Particularly, the presence of the acetonitrile group was confirmed by the singlet peak at $\delta = 1.29$ ppm in the ^1H NMR spectrum, and also by the stretching of the C≡N bond at 2309 cm^{-1} in the IR analyses. MS spectrum confirmed the formation of the product, by the peak at m/z 471.1331, corresponding to the nickel complex plus H^+ ion ($[M+H]^+$, $C_{25}H_{25}N_4NiO_2^+$). Finally, Uv-vis spectrum of **13**, was found to be similar to that of **10**. Indeed, the main peak (at $\lambda_1 = 333$ nm) and the shoulder (at $\lambda_2 = 430$ nm) appeared just slightly shifted to the left compared to that of **10**.

2.1.5 Ligand exchange reactions

As described above (paragraph 2.1.4), thanks to the presence in **13** of the labile acetonitrile group, three ligand exchange reactions were carried out with $[Et_4N][OC(O)CH_3]$, $[Et_4N][Cl]$, $[Et_4N][OC(O)H]$ affording the anionic complexes, $[Et_4N][Ni^{II}(pyN_2^{Me2})(OC(O)CH_3)]$ (**15**), $[Et_4N][Ni^{II}(pyN_2^{Me2})(Cl)]$ (**20**) and $[Et_4N][Ni^{II}(pyN_2^{Me2})(OC(O)H)]$ (**22**) respectively (Figure 22). All these nickel complexes were characterized by ^1H NMR, IR and UV-vis spectroscopies. Moreover, we obtained the molecular structure of **15**, since its crystals were found to be suitable for X-ray diffractometry.

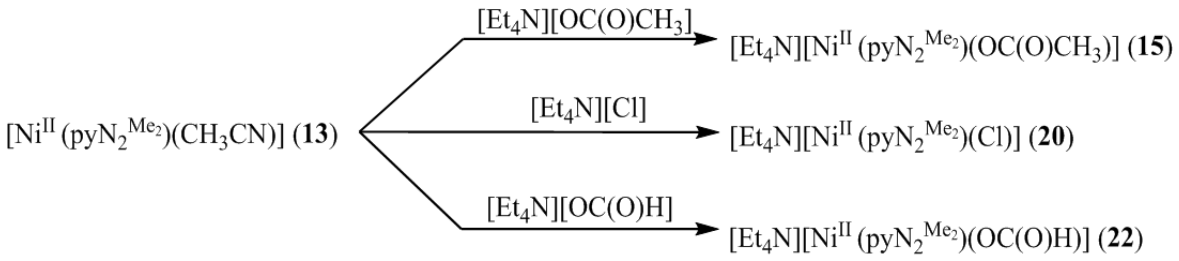

Figure 22. Ligand exchange reactions from [$Ni^{II}(pyN_2^{Me2})(CH_3CN)$] (**13**)

After the characterization, **15** and **22** were reacted with one-electron oxidants giving the Ni(III) compounds [$Ni^{III}(pyN_2^{Me2})(OC(O)CH_3)$] (**18**) and [$Ni^{III}(pyN_2^{Me2})(OC(O)H)$] (**25**) whose reactivity was further investigated in OAT and HAA reactions (see section 2.2). The reactivity of complex **20** was not investigated because it does not contain a Ni-O bond. **18** and **25** were also obtained using **10** as starting material. In particular, **10** was reacted with NaOCl/Acetic acid and NaOCl/Formic acid respectively (see section 2.2). Nonetheless, the results obtained by this procedure, for both complexes, turned out to be less accurate than those obtained by employing [$Ni^{II}(pyN_2^{Me2})(CH_3CN)$] (**13**) as starting complex.

Regarding the Uv-vis spectrum of these Ni compounds, we noticed that those bearing a Ni-O bond (**10**, **15**, **22**) were characterized by the same electronic absorption features. Indeed, **15** and **22**, bearing a carboxylate group, showed the same Uv-vis spectrum of **10**, featured by a bicarbonate ligand, with a strong absorption at λ_1 = 380 nm and a shoulder at λ_2 = 475 nm (section 2.2: Figure 2). Conversely, **20**, binding a chloride atom, displayed a completely different UV-vis spectrum compared to the other species (**10**, **15**, **22**). In particular, it showed two main peaks at λ_1 = 390 and λ_2 = 460 nm and a weaker absorption feature at λ_3 = 500 nm.

Regarding the MS analysis, it confirmed the formation of **15**, **20**, **22**, showing the peaks of such anionic compounds [M^-] respectively at m/z 488.1128 ($C_{25}H_{24}N_3NiO_4^-$), 464.0980 ($C_{23}H_{21}ClN_3\ NiO_2^-$) and 474.0982 ($C_{24}H_{22}N_3\ NiO_4^-$). Moreover, the presence of the acetate and formate group in compounds **15** and **22** were detected by the ^{1}H NMR spectra. They displayed a singlet peak at δ = 0.73 and δ = 7.10 ppm respectively.

Finally, regarding the single-crystal X-ray analyses of **22** (Figure 23), it showed a nickel ion in a square planar environment coordinated to three N-donors, from the pincer ligand pyN_2^{Me2}, plus an acetate group in the fourth coordination site, as well as a water molecule

and the tetraethylammonium counter ion. The acetate group is bound in a monodentate manner via a single oxygen atom, and is perpendicular to the plane of the pincer ligand.

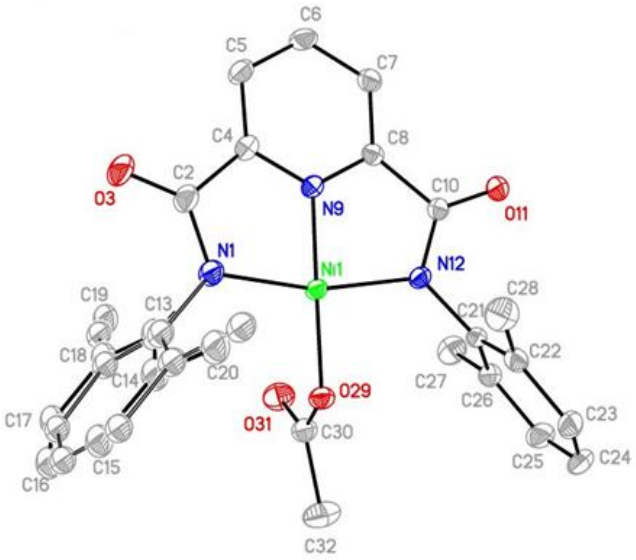

Figure 23. Solid-state structure of **22** ; the hydrogen atoms, the water molecule and the tetraethylammonium counter ion are not depicted for simplicity.

2.2 Synthesis of Ni(III) complexes

2.2.1 Introduction

The Ni(II) complexes described in section 2.1 were oxidized under suitable conditions affording the related Ni(III) complexes. These oxidized species, in turn, were investigated in the oxygen atom transfer (OAT) and hydrogen atom abstraction (HAA) reactions which are typical of biological high-valent metal-oxygen species. Particularly, HAA and OAT reactions were performed by adding 2,6-di-tert-butylphenol (2,6-DTBP) at -40 °C, and triphenylphosphine (PPh_3) at -80 °C, respectively. Overall, we carried out the synthesis of the high-valent nickel-oxygen complexes [$Ni^{III}(py{N_2}^{Me2})(OCO_2H)$] (**12**), [$Ni^{III}(py{N_2}^{Me2})(ONO_2)$] (**14**), [$Ni^{III}(py{N_2}^{Me2})(OC(O)CH_3)$] (**18**) and [$Ni^{III}(py{N_2}^{Me2})(OC(O)H)$] (**25**). The reactivity of **12** has been studied in a previous work, therefore we only investigated that of **14**, **18**, **25** and finally compared the behavior of all the four species. In particular, the reactivity of the Ni(III) species, was investigated by reacting the complexes with 7 to 500 equivalents of substrate to ensure pseudo-first order conditions. After, the values for the observed k_{obs} were obtained by fitting the decay of the absorbance, at the main electronic absorption, against time as an exponential. Finally, the second-order rate constants (k_2) were calculated by repeating the determination with varying concentrations of substrate. Still, the value of k_2 of the three species were compared and results are discussed in the following sections.

2.2.2 Synthesis of $[Ni^{III}(pyN_2^{Me2})(OCO_2H)]$ (12)

The Ni(III) complex **12** was obtained by oxidation of **10** (Figure 24) which synthesis is described in the previous section 2.1.2.

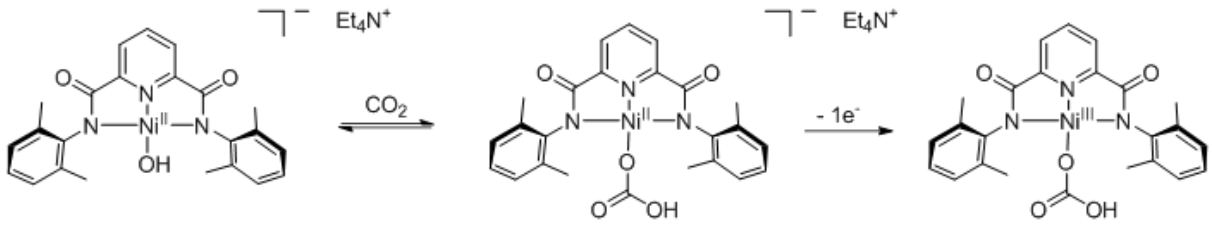

(8) **(10)** **(12)**

Figure 24. Interconversion between **8** and **10** and oxidation **10** to **12.**

10 is quantitatively transformed into **12** by adding 1 equivalent of the organic oxidant Tris(4-bromophenyl)ammoniumyl hexachloroantimonate ("Magic Blue", dissolved in CH_3CN, $E°' = 0.70$ V vs. Fc^+/Fc). **12** shows two electronic absorption features: the first more intense at $\lambda_1 = 520$ nm and the second weaker at $\lambda_2 = 790$ nm (black trace Figure 2). They can be assigned as charge transfer bands to the metal. Conversely, the parent complex **10** (as described in section 2.1.2) displays a strong absorption at $\lambda_1 = 380$ nm and a shoulder at $\lambda_2 = 475$ nm (grey trace Figure 25 a). Thus, Uv-vis spectroscopy clearly indicates that **10** is quantitatively transformed into **12**. The reaction stoichiometry 1:1 between **10** and Magic Blue, suggested the formulation of **12** as a one-electron oxidised Ni(III) species, retaining the same ligand of **10**. Moreover since **12** was thermally unstable, the best conditions for the oxidation process were found to be in acetone at -80°C, monitored by UV-vis Spectroscopy. Even at this very low temperature, the oxidation process is very fast and **10** is quantitatively transformed into **12** in a few seconds after the addition of the oxidant (Figure 25 a). **12** was also characterized by EPR spectroscopy. In particular, the spectrum (Figure 25 b) displayed a distinct magnetic anisotropy that was indicative of an approximate axial symmetry ($g_\perp = 2.25$, $g_{//} = 2.02$). Moreover, $g_\perp$ was greater than $g_{//}$, which for Ni(III) complexes is typical of axially elongated octahedral or square planar coordination;[40,41,42–47] the square planar geometry was thus maintained after the oxidation.

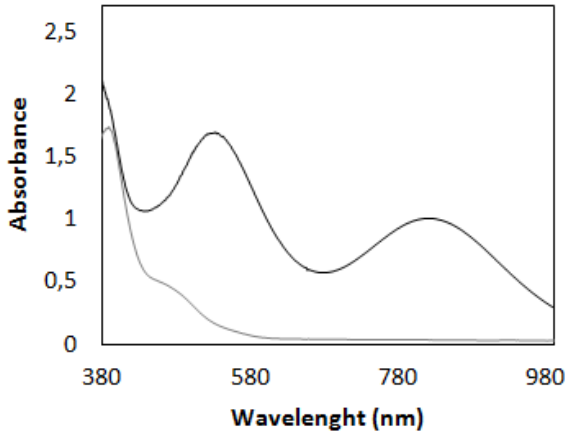

(a)

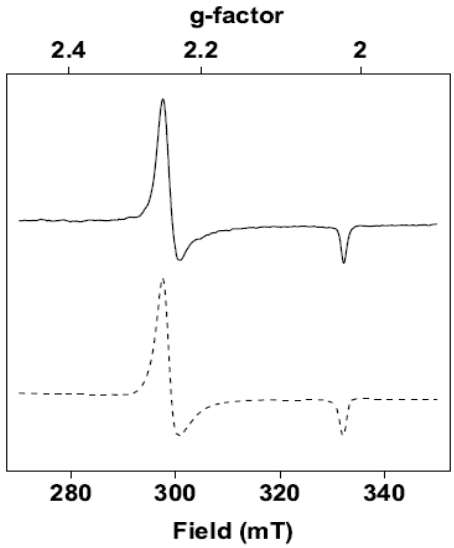

(b)

Figure 25a. UV spectrum of **10** (grey trace t = 0 s) reacted with 1 equivalent of Magic Blue at -80°C to yield **12** (black trace t = 12 s).

Figure 25b. Solid trace: X-band EPR spectrum of a frozen solution of **12**. Dashed trace: simulated spectrum.

As describe above (paragraph 2.2.1), the HAA and OAT reactivity of complex **12** has been studied in a previous work. Particularly, during that work, the values for the observed rate constants (k_{obs}) were obtained by fitting the change in absorbance at 520 nm (the first and more intense feature of **12**) against time as an exponential. Then, the values of the second-order rate constant k_2 = 0,1033 s^{-1} and k_2 = 5,1515 s^{-1} were calculated by repeating the determination with varying concentrations of 2,6-DTBP and PPh_3, respectively. Regarding our work, it was only investigated how to improve the synthesis of **12** by using an alternative oxidant to magic blue, as described in the following paragraph 2.2.2.1.

2.2.2.1 Alternative oxidant to Magic Blue

Since Magic Blue turned out to be difficult to handle because oxygen and light sensitive, another oxidant was tested for the oxidation of **10**: 1,1'-dibenzoyl ferrocenium hexafluorophosphate (Figure 26).

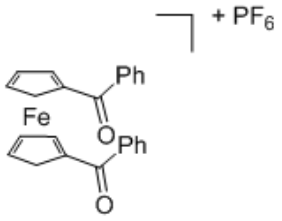

Figure 26. Structure of 1,1'- dibenzoyl ferrocenium hexafluorophosphate

The use of this oxidant resulted in the formation of **12** in lower yields compared to Magic blue, as determined by UV-vis spectroscopy. Indeed **12,** upon its formation, showed a partial decay during which its peak intensity decreased in few seconds without disappearing completely (Figure 27). This partial decay was probably promoted by the presence of iron in the reaction mixture. That hypothesis was supported by the rapid decay of the iron-based oxidant solution that was found not to be stable, switching from dark green to brown in 4-5 minutes. Overall, 1,1'-dibenzoyl ferrocenium hexafluorophosphate was capable to oxidize **10** and give **12** but not suitable for the reactivity studies because of its fast decay in solution and the low yield of the Ni(III) complex obtained. Thus, magic blue remains the best oxidant for the preparation of **12** and its reactivity studies.

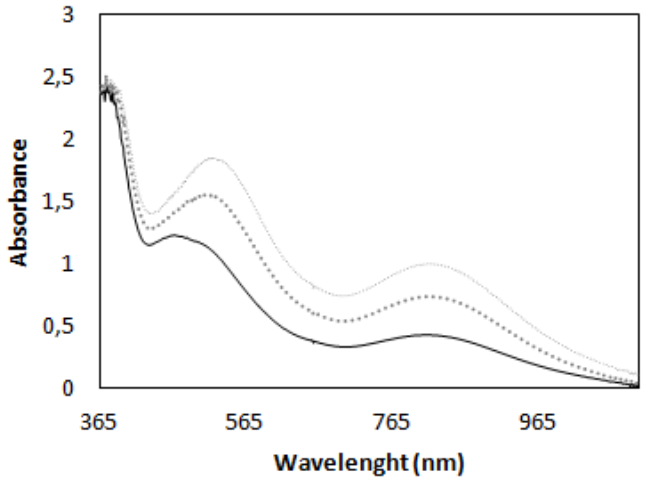

Figure 27. Uv-vis spectrum of **12** obtained by reacting **10** with 1 equivalent of 1,1'-dibenzoyl Ferrocenium hexafluorophosphate at -80 °C. Dashed gray traces (t = 0 s; t = 2 s): Ni(III) complex decay. Black solid trace (t = 10 s): stable Ni(III) complex.

2.2.3 Synthesis and reactivity of $[Ni^{III}(pyN_2^{Me2})(ONO_2)]$ (14)

(10) **(14)**

Figure 28. Reaction between **10** and CAN to yield **14**

14 was obtained by reaction of **10** (dissolved in acetone) with the inorganic oxidant ammonium cerium(IV) nitrate $[NH_4]_2[Ce(NO_3)_6]$ (CAN) (dissolved in methanol) at low temperature (T = - 80 °C) (Figure 28). After reacting **10** with 6 equivalents of CAN a new species **14** was formed, with two electronic absorption features: the first and more intense at λ_1 = 580 nm and the second less intense at λ_2 = 900 nm (Figure 29). Regarding the reaction mechanism, we may supposed that first CAN oxidizes **10** affording the Ni(III) complex **12**. Then, HCO_3^- is replaced by NO_3^- resulting in **14**. Probably the substitution step is favoured by protonation of the bicarbonate ligand by the NH_4^+ ions present in CAN and the presence of a large excess of NO_3^- ions.

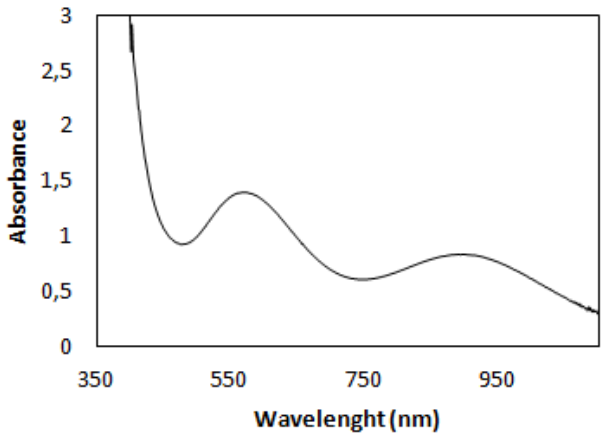

Figure 29. UV-vis spectrum of **14** obtained by reacting **12** with 6 equivalents of CAN at -80 °C.

14 was obtained in lower yields compared to **12**. The two electronic absorption features of **14** (λ_1 = 580 nm and λ_2 = 900 nm) can be tentatively assigned as charge transfer bands (LMCT) to the now electron-poorer metal centre, in the view of the replacement of HCO_3^- with the more electron withdrawing NO_3^-. The oxidation state of the metal centre was definitely confirmed by the EPR analyses. An axial EPR spectrum (Figure 30) ($g_\perp$ = 2.25, $g_{//}$ = 2.02), very similar to that of **12**, was recorded for this new species and the similarities in the UV-vis and EPR spectra have led us to formulate **14** as the Ni(III) Nitrate complex $[Ni^{III}(pyN_2^{Me2})(ONO_2)]$ (**14**), isostructural with **12**.

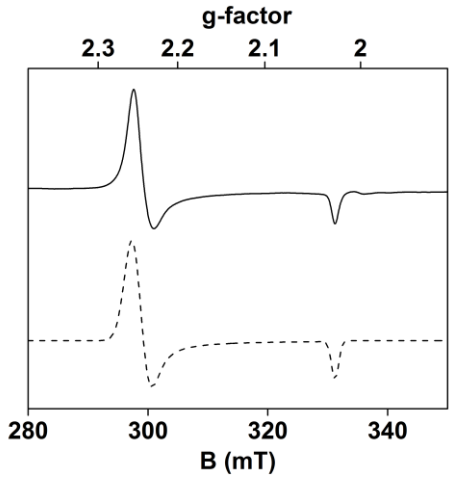

Figure 30. Solid trace: X-band EPR spectrum of a frozen solution of **14**. Dashed trace: simulated spectrum.

2.2.3.1 Reaction of [$Ni^{III}(pyN_2^{Me2})(ONO_2)$] (14) with PPh_3

The OAT reactivity of **14** was investigated by addition of PPh_3 to a freshly prepared solution of the Ni(III) complex in acetone at - 80°C. The reaction with this substrate was very fast and the reduction of Ni(III) to Ni(II) (Figure 31) was observed in the UV-spectrum suggesting that the complex reacted and oxidized PPh_3 to triphenylphosphineoxide ($OPPh_3$) as observed via mass spectrometry.

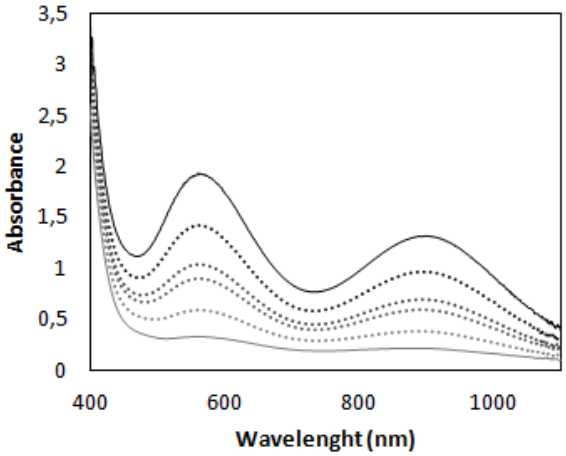

Figure 31. Spectral changes, recorded at different times, observed by reacting **14** (black solid trace t = 0 s) with PPh_3 (4 equivalents) at – 80 °C. Grey solid trace: end-of reaction mixture (t = 5 s).

The disappearance of the features of **14** in the UV-vis spectrum, after adding PPh_3, confirms that **14** may oxidise the substrate being reduced to Ni(II). Nonetheless $OPPh_3$ may be in part formed also by reaction of PPh_3 with CAN, as verified in a blank test at RT in the absence of **14**. Therefore, the kinetic constant for the OAT reaction between **14** and PPh_3 was determined based on the decay of the UV-vis features of **14** which was not affected by the side reaction between CAN and PPh_3. Indeed, values for the observed rate constant (k_{obs}) were obtained by fitting the change in absorbance at 580 nm (the first and more intense feature of **14**) against time as an exponential. Then, the second-order rate constant (k_2 = 0,4046 $M^{-1}s^{-1}$) was calculated by repeating the determination with varying concentrations of PPh_3 (Figure 32).

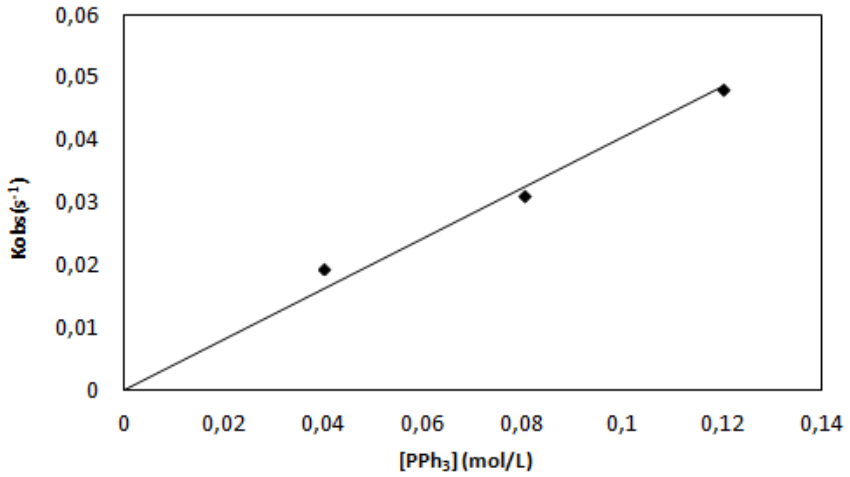

Figure 32. Plots of k_{obs} versus [PPh_3] obtained for the reaction between **14** and PPh_3 at - 80°C.

2.2.3.2 Reaction of [$Ni^{III}(pyN_2^{Me2})(ONO_2)$] (14) with 2,6-DTBP

In order to probe the HAA reactivity of **14**, we reacted it with 2,6-DTBP at - 40°C . Unfortunately at this lower temperature **14** was not much stable and, thus, it was formed in lower yields and it rapidly decomposed, hampering the HAA studies.

In order to obtain **14** in higher yield and, consequently, a greater reproducibility of k_{obs}, the number of equivalents of CAN was reduced (from 6 to 4). In this way the stability of **14** was found to be higher. Then, many tests with different concentrations of the substrates were carried out. Thanks to these changes, the decay turned out to be negligible compared to HAA reaction, and a second-order rate constant could be calculated (k_2 = 0.748 $M^{-1}s^{-1}$) (Figure 34). The occurrence of the HAA reaction was confirmed by mass spectrometry where evidence of 2,6-di-tert-butyl-1,4-benzoquinone (**16b**, Figure 33) and of 3,3',5,5'-tetra-tert-butyl-[1,1'-biphenyl]-4,4'-diol (**16c,** Figure 33) was found**.** Particularly, **16b** derived from the oxidation of the monoradical (**16a**), which was generated by one-electron reduction of [$Ni^{III}(pyN_2^{Me2})(ONO_2)$] **14** to Ni(II). Conversely, **16c** derives from the coupling of the monoradical **16a** (Figure 33).

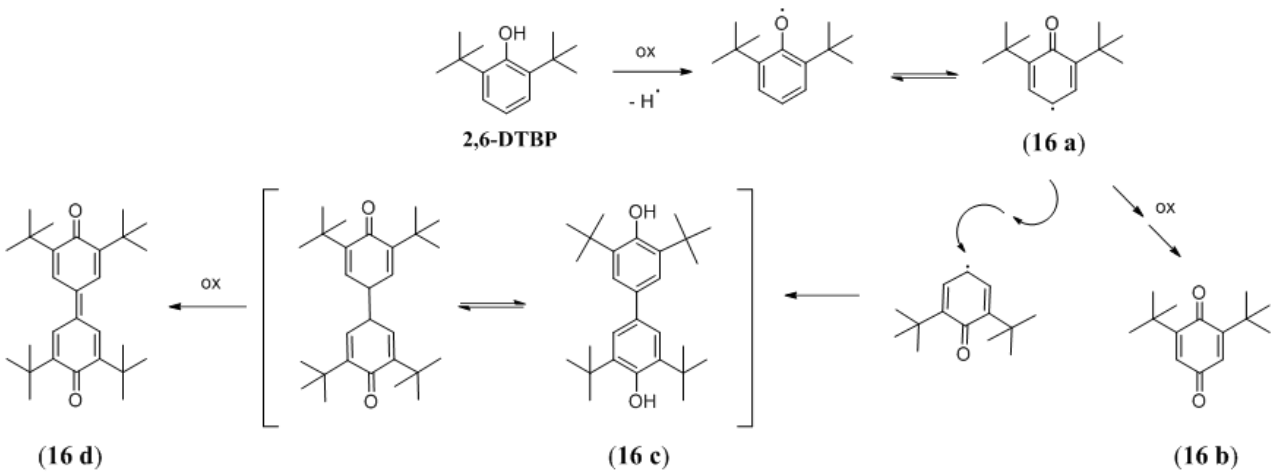

Figure 33. Formation of the final products from the oxidation of 2,6-DTBP via HAA.

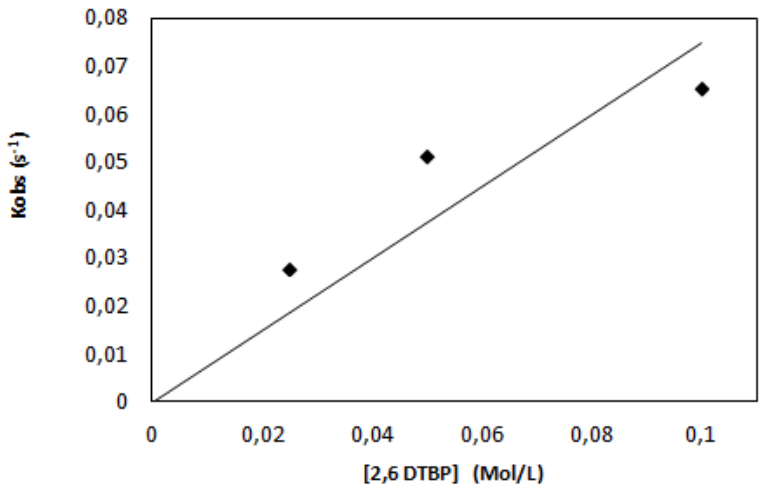

Figure 34. Plots of k_{obs} versus [2,6-DTBP] determined for the reaction between **14** and 2,6-DTBP at -40 °C.

2.2.3.3 Reaction of [$Ni^{III}(pyN_2^{Me2})(ONO_2)$] (14) with 2,4-di-tert-butylphenol (2,4-DTBP)

In order to study the behaviour of **14** with a less hindered di-tert-butylphenol, we reacted it with 2,4-ditert-butylphenol (2,4-DTBP) at -40 °C. The reaction was found to be much faster than that carried out with 2,6-DTBP at the same temperature. Occurrence of HAA reaction was confirmed by mass spectrometry analyses, where we found evidence of the radical coupling product 2,4-ditert-butyl-6-(2,4-ditert-butyl-5-oxidanyl-phenyl)phenol (Figure 35).

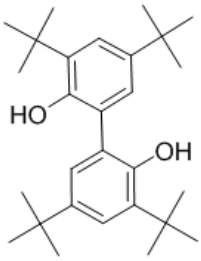

Figure 35. Structure of the radical coupling product: 2,4-ditert-butyl-6-(2,4-ditert-butyl-5-oxidanyl-phenyl)phenol

As described above (paragraph 2.2.3.1), values for the observed rate constant (k_{obs}) were obtained by fitting the decay of the absorbance at 580 nm against time as an exponential. By repeating the determination with varying concentrations of 2,4-DTBP, a second-order rate constant has been calculated: k_2 = 8.474 $M^{-1}s^{-1}$ (Figure 36). This value of k_2 is one order of magnitude greater than that found in the reaction with 2,6-DTBP (k_2 = 0.748 $M^{-1}s^{-1}$). Thus, using a less hindered substrates makes the reaction considerably faster.

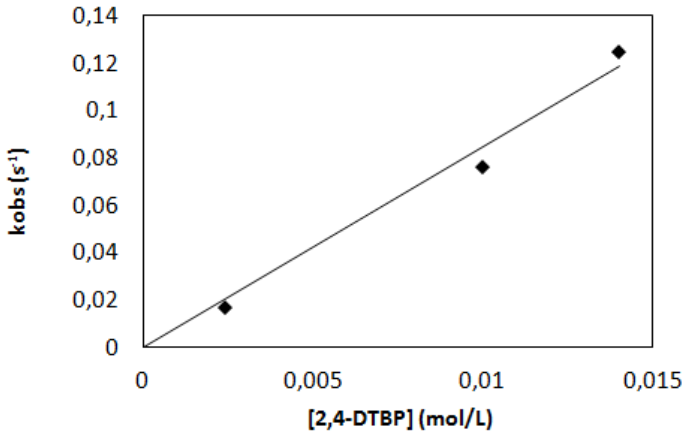

Figure 36. Plots of k_{obs} versus [2,4-DTBP] determined for the reaction between **14** and 2,4-DTBP at -40 °C.

2.2.4 Synthesis and reactivity of $[Ni^{III}(pyN_2^{Me2})(OC(O)CH_3)]$ (18)

$$[Ni^{II}(pyN_2^{Me2})(OCO_2H)]^- \xrightarrow[CH_3COOH]{NaOCl} [Ni^{III}(pyN_2^{Me2})(OCOCH_3)]$$

(10) **(18)**

Figure 37. Generation of **18** by reacting **10** with an oxidizing mixture made up of NaOCl and CH_3COOH.

18 was obtained by reaction between **10** and an oxidizing mixture made up of NaOCl and CH_3COOH at low temperature (T= - 80 °C) (Figure 37). In the oxidizing mixture NaOCl oxidized the metal centre and CH_3COOH provided the acetate group during the reaction and creates an acidic environment that increases the NaOCl oxidizing power. The Ni(III) complex **18** shows two electronic absorption features similar to **12**: the first and more intense at λ_1 = 520 nm and the second less intense at λ_2 = 750 nm. Since NaOCl was not soluble in acetone (the solvent used to make the **10** solution), upon the addition of the oxidizing mixture a precipitate was formed, causing light dispersion and compromising the reactivity studies. Since **18** was found to be quite stable at room temperature, the problem was solved by filtering the solutions. In addition, before recording the UV-vis spectra, **18** was characterized by EPR analyses and it showed an axial EPR spectrum ($g_\perp$ = 2.24, $g_{//}$ = 2.02), very similar to **12** (Figure 38).

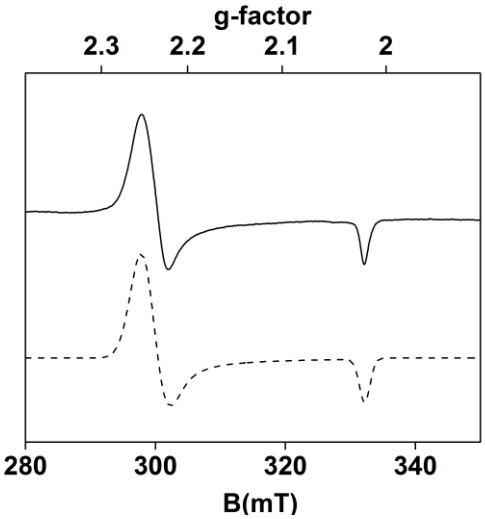

Figure 38. Solid trace: X-band EPR spectrum of a frozen solution of **18**. Dashed trace: simulated spectrum.

2.2.4.1 Reaction of [$Ni^{III}(pyN_2^{Me2})(OC(O)CH_3)$] (18) with PPh_3

In order to investigated the OAT reactivity of **18**, we reacted it with triphenylphosphine at -80 °C. Upon the addition of PPh_3 to **18,** we noticed only slight changes in the Uv-vis spectrum (Figure 39), without the appearance of the typical Ni(II) absorption features as in the other cases. Such behaviour led us to suppose that no change occurred in the oxidation state of the metal. In particular, it is likely that a ligand exchange reaction took place instead of the expected redox reaction. Indeed, the Ni(III) in complex **18** could have bonded the PPh_3 maintaining the same oxidation state. Because of these complications, we did not carry out any further study on this reaction.

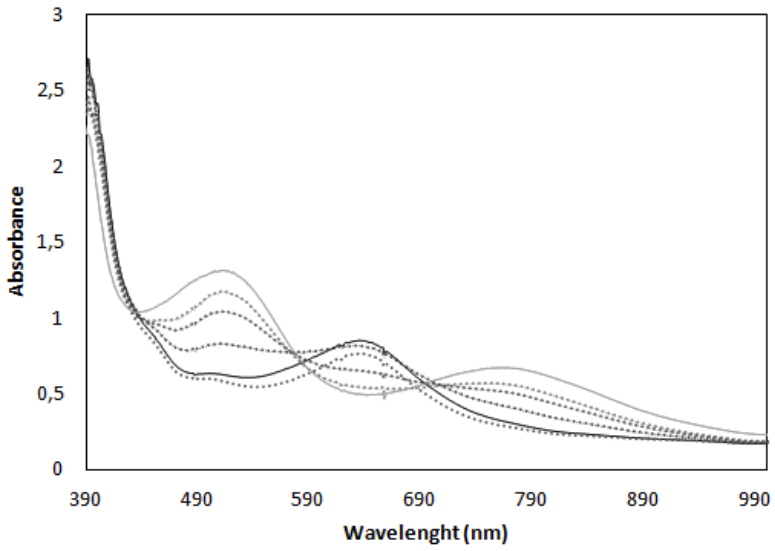

Figure 39. Uv-vis spectral changes occurred upon the reaction of **18** (solid grey trace t = 0 s) with 250 equivalents of PPh_3 at - 80 °C. Black solid trace: end-of reaction mixture (t = 320 s)

2.2.4.2 Reaction of [$Ni^{III}(pyN_2^{Me2})(OC(O)CH_3)$] (18) with 2,6-DTBP

In order to probe the HAA reactivity of **18,** we reacted it with 2,6-DTBP at -40 °C. Regarding this reaction, we had some initial troubles finding out the correct experimental conditions, since this reaction was too slow and the values of k_{obs} obtained, by fitting the decay of the absorbance at 520 nm against time as an exponential, were not accurate. In

order find the best conditions, we did different attempts changing the amount of 2,6-DTBP and the NaOCl:CH_3COOH ratio, but the results obtained were unsatisfactory. Eventually, great improvements were obtained changing the starting Ni(II) complex from the bicarbonate complex **10** to the acetate **15** (Figure 40). Indeed, **15** was oxidized (with the NaOCl/CH_3COOH mixture) instead of **10,** affording **18** which was finally reacted with 2,6-DTBP.

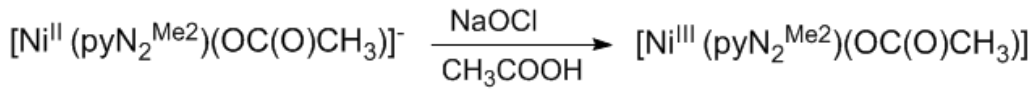

(15) **(18)**

Figure 40. Generation of the Ni(III) complex **18** by reacting **15** with an oxidizing mixture made up of NaOCl and CH_3COOH

In this way, the values of k_{obs} obtained by fitting the decay of the absorbance at 520 nm against time as an exponential, were accurate. After, by plotting k_{obs} versus different values of 2,6-DTBP concentration (Figure 41)**,** the second-order rate constant (k_2 = 0.1103 $M^{-1}s^{-1}$) has been calculated.

Regarding the initial troubles related to this reaction, we supposed that most likely the improvements obtained by the employment of **15** are due to the fact that it led to a purer solution compared to the one obtained by using **10**. Indeed, the latter was probably a mixture of **12** and **18** and the presence of **12** could have compromised the reproducibility of k_{obs}. This, in turn, arises from the fact that, by using **10**, ligand exchange is not complete and, after oxidation, a mixture of bicarbonate (**12**) and acetate (**18**) is present. Conversely, under the same experimental conditions, **15** is quantitatively oxidized to **18**, since they both contain the same ligands.

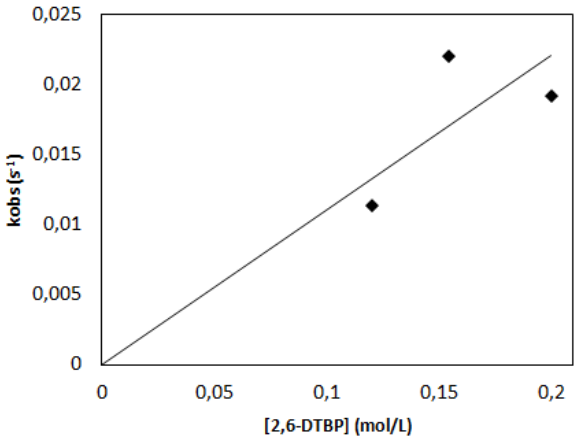

Figure 41. Plots of k_{obs} *v*ersus **[**2,6-DTBP**]** determined for the reaction between **18** and 2,6-DTBP at -40 °C

Evidence of the coupling product 3,3',5,5'-tetra-tert-butyl-4,4'diphenoquionone (**16d**, Figure 33) was found in the NMR and UV-vis spectrum of the end-of-reaction mixture. In the UV-vis spectrum, that coupling product was confirmed by the weak signal at 421 nm (circled area Figure 42).

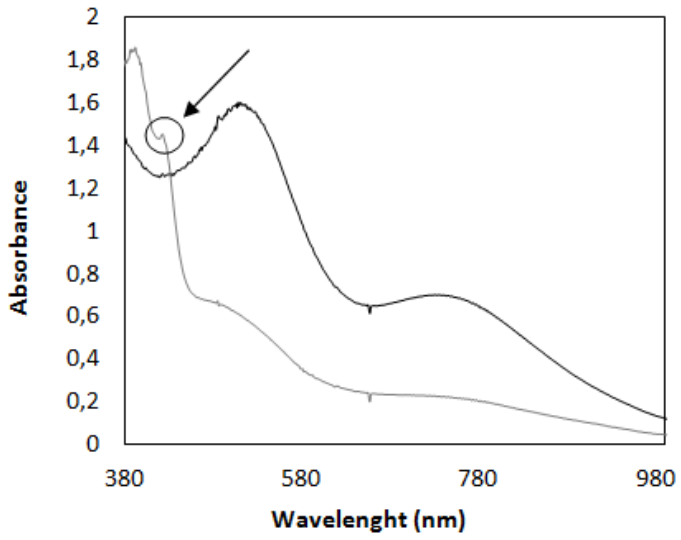

Figure 42. UV-vis spectral changes in the reaction of **18** (black trace t = 0 s) with 300 equivalents of 2,6-DTPB at - 40 °C. The final mixture (grey trace t = 60 s) showed the weak signal of the coupling product **16d** at 421 nm (circled area).

The Uv-vis spectrum of the final mixture, obtained after the reaction of **18** with 2,6-DTBP, presented the typical electronic absorption features of the starting Ni(II) complex

15 with a main peak at λ_1 = 380 nm and a shoulder at λ_2 = 475 nm (grey trace Figure 42). Therefore, during the HAA reactions, the Ni (III) metal centre of complex **18** should be reduced to Ni(II) maintaining the same monodentate ligand -$OC(O)CH_3$. Interestingly, **18** showed the same behaviour also in the other HAA reactions performed with phenol and di-methyl-phenol (see sections 2.2.4.4 and 2.2.4.5). Conversely, as described above (paragraph 2.2.4.1), the OAT reaction performed reacting **18** with PPh_3, resulted in only slight changes in the Uv-vis spectrum without the appearance of the typical Ni(II) absorption features. Indeed, in this case, it was supposed a ligand exchange reaction with PPh_3 instead of the of the expected redox reaction.

2.2.4.3 Reaction of [$Ni^{III}(pyN_2^{Me2})(OC(O)CH_3)$] (18) with other substrates for HAA reaction

In the following sections (2.2.4.4 and 2.2.4.5) we decided to further explore the HAA reactivity of **18** by reacting it with other substrates different from 2,6-DTBP, such as 2,6-dimethyl-phenol and phenol. In both cases the reaction was monitored by UV-vis spectroscopy. Then, we set out to investigate the behaviour of **18** with cycloalkenes such as 1-methylcyclohexa-1,4-diene and cyclohexene. In this cases, **18** was expected to perform the epoxidation of the cycloalkenes. We did several attempts but **18** seemed not to be reactive towards these last two compounds. Then, in the following sections we will describe in details only the reactions with 2,6-dimethyl-phenol and phenol.

2.2.4.4 Reaction of [$Ni^{III}(pyN_2^{Me2})(OC(O)CH_3)$] (18) with 2,6-di-methyl-phenol

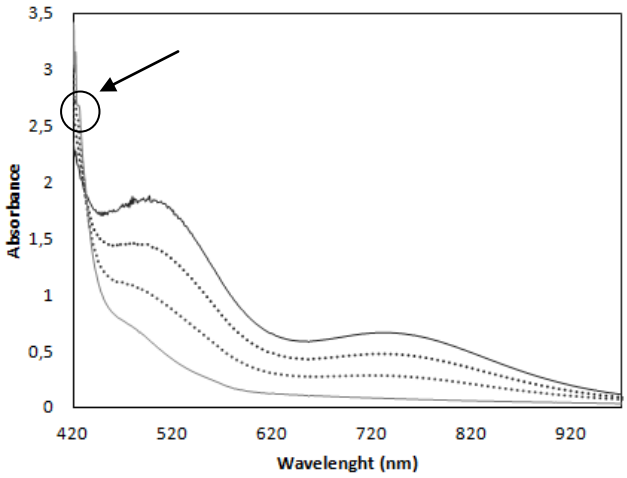

Figure 43. Uv-vis spectral changes produced upon reaction of **18** (solid black trace t = 0 s) with 1 equivalent of 2,6-dimethyl-phenol at -40 °C. The end-of reaction mixture (solid grey trace t = 5s) showed the weak signal of the coupling product **21** at 421 nm (circled area)

Reacting **18** with 2,6-dimethyl-phenol (at – 40°C), Ni(III) was reduced to Ni(II) as evidenced by Uv-vis spectroscopy (Figure 43). Since this reaction was found to be very fast, it was performed by adding just one equivalent of substrate. Moreover, occurrence of HAA reaction was confirmed by the signal of the coupling product 3,3',5,5'-tetra-methyl-4,4'diphenoquionone (**21**, Figure 44) in the UV-vis spectrum recorded at the end of the reaction (weak peak in the solid grey trace around 420 nm, circled area Figure 43). Afterwards, the presence of the coupling product **21** was also confirmed by ^{1}H NMR analyses.

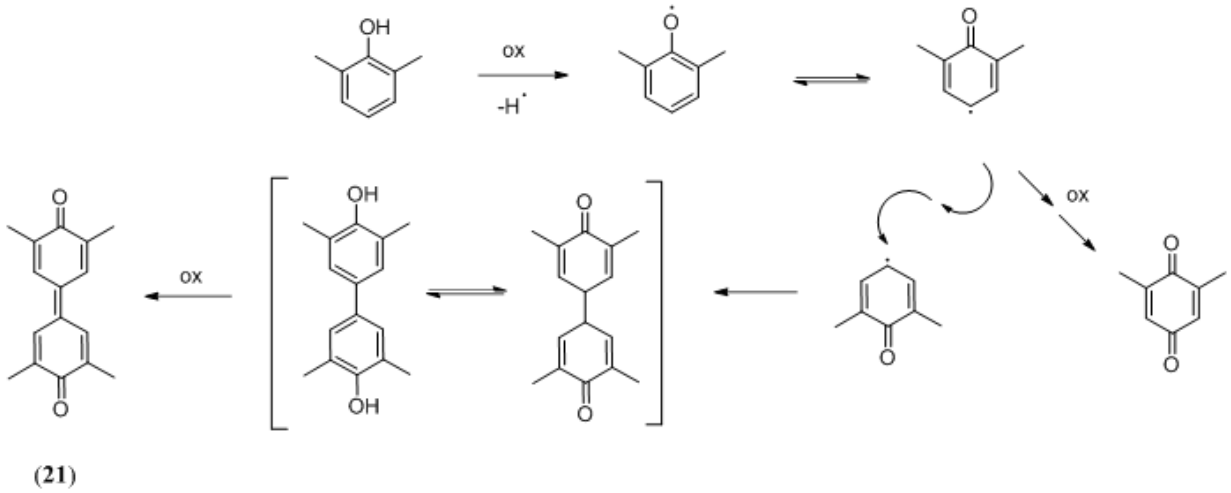

Figure 44. Formation of the final products from the oxidation of 2,6-dimethyl-phenol via HAA at -40 °C

2.2.4.5 Reaction of [$Ni^{III}(pyN_2^{Me2})(OC(O)CH_3)$] (18) with phenol

By reacting **18** with phenol at -40 °C, Ni(III) was reduced to Ni(II). Unfortunately it was not possible to identify the nature of the product of oxidation of phenol by NMR and mass spectrometry. We supposed, that the first step of the reaction should have been the same of the one with 2,6-DTBP but most likely during the second step the radical did not form the coupling product but another compound with a different structure which is unknown. Future work will be dedicated to this issue.

2.2.4.6 Synthesis and reactivity of [$Ni^{III}(pyN_2^{Me2})(OC(O)H)$] (25)

Since [$Ni^{III}(pyN_2^{Me2})(OC(O)CH_3)$] **(18)** showed to be reactive with many substrates, we set out to investigate the HAA and OAT reactivity of another Ni(III) complex with a carboxylate ligand ($RCOO^-$) in the fourth coordination position. In particular, we studied the Ni(III) complex [$Ni^{III}(pyN_2^{Me2})(OC(O)H)$] (**25**) with a formate ion binding the metal centre. The procedure performed for the synthesis of **25** was the same of **18**. Initially, **10** was reacted with an oxidizing mixture made up of NaOCl and formic acid. Afterwards, in order to increase the yield of **25**, we decided to use as starting material [$Ni^{II}(pyN_2^{Me2})(OC(O)H)$] (**22**), and oxidize it instead of **10**. Once obtained **25** in high

yield we reacted it with PPh_3 and 2,6-DTBP but the results haven't been successful. Indeed, the Ni(III) complex was found not to be reactive towards both substrates.

2.2.5 Discussion of the rate constants and potential mechanisms

2.2.5.1 Reaction of oxygen atom transfer (OAT)

The results obtained by reacting the Ni(III) complexes **12**, **14**, **18**, **25** with PPh_3 **(**at – 80 °C), in order to investigate their OAT reactivity, will be discussed in this paragraph. The first two complexes [$Ni^{III}(pyN_2^{Me2})$ (OCO_2H)] (**12**) and [$Ni^{III}(pyN_2^{Me2})$ (ONO_2)] (**14**) showed to be reactive towards PPh_3 and the second-order rate constants (k_2) have been calculated (Figure 45).Conversely, **18** and **25** were not reactive towards triphenylphosphine.

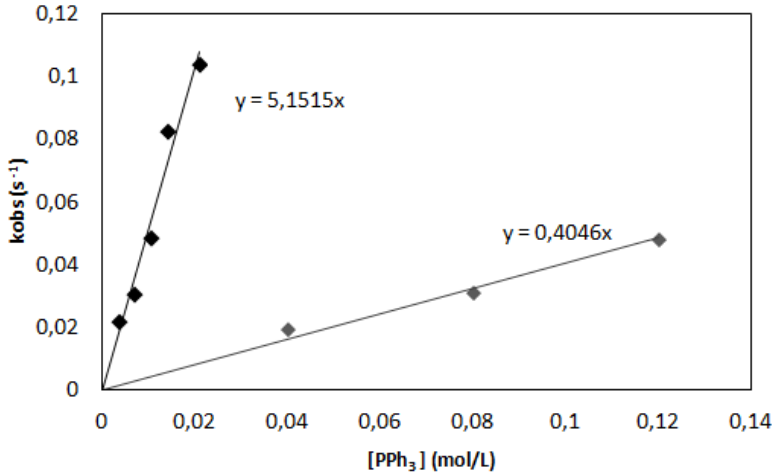

Figure 45. Plots of k_{obs} versus [PPh_3] determined for the reaction between **12** and PPh_3 (black) and for the reaction between **14** and PPh_3 (grey).

By comparing the values of the second-order rate constants obtained, **12** (k_2 = 5,1515 $M^{-1}s^{-1}$) was found to be more reactive towards PPh_3 than **14** (k_2 = 0,4046$M^{-1}s^{-1}$). According to this comparison we supposed a concerted mechanism (OAT) for **12**, where PPh_3 attacks the oxygen binding the metal centre, promoting the breakage of C-O bond and the

reduction of Ni(III) to Ni(I) (Figure 46). Ni(I) is unstable and probably oxidized to Ni(II) at the end of the reaction. Indeed electronic absorption features typical of a Ni(II) complex were found in the UV-vis spectra at the end of the reaction.

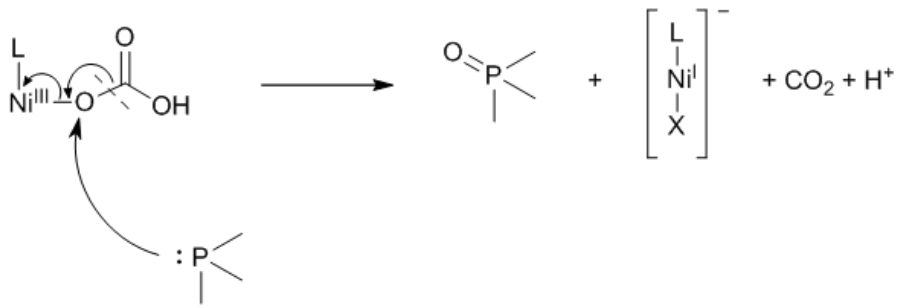

Figure 46. Proposed reaction mechanism for OAT performed by adding PPh_3 to **12**

The proposed concerted mechanism, is also supported by the fact that $[Ni^{III}(pyN_2^{Me2})(OC(O)CH_3)]$ (**18**) and $[Ni^{III}(pyN_2^{Me2})(OC(O)H)]$ (**25**) containing a carboxylate ligand instead of a bicarbonate and nitrate group, are not reactive towards PPh_3. Likely, the reaction of **18** and **25** with PPh_3 is not favoured, because the cleavage of the bond between the oxygen atom binding the metal and the carbonyl carbon atom is not energetically affordable in carboxylic acids (Figure 47).

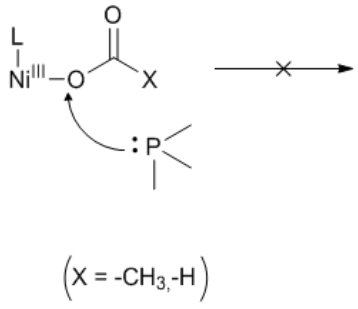

Figure 47. Ni(III) complexes with a carboxylate ligand were found not to be reactive towards PPh_3.

Finally, since **14** was found to be less reactive compared to **12** and more reactive compared to **18** and **25**, we suppose that the reaction between **14** and PPh_3 could have followed either an OAT or an electron transfer (ET) mechanism. Indeed, the cleavage of the N-O bond within the nitrate group, could have been energetically more accessible compared to that within the carboxylic group, but not as favoured as that within the

bicarbonate group. Overall, the data collected by reacting different Ni(III) complexes (**12**, **14**, **18**, **25**) with PPh_3 led us to conclude that the mechanism could depend on the nature of the ligand binding the metal centre.

2.2.5.2 Reaction of hydrogen atom abstraction (HAA)

The HAA reactivity of Ni(III) complexes of the type $[Ni^{III}(pyN_2^{Me2})(X)]$, was investigated by reacting them with 2,6-DTBP at - 40 °C. **12**, **14**, **18** were reactive towards that substrate and a the second-order rate constant (k_2) was determined for each nickel species. Moreover, interesting data was collected by reacting **14** with a less hindered di-tert-butylphenol, 2,4-DTBP. Indeed, as shown in the following graph (Figure 48), the second-order rate constant obtained for the reaction of **14** with 2,4-DTBP (k_2 = 8.474 $M^{-1}s^{-1}$) was almost 10 times greater than that obtained by reacting **14** with 2,6-DTBP (k_2 = 0.748 $M^{-1}s^{-1}$).

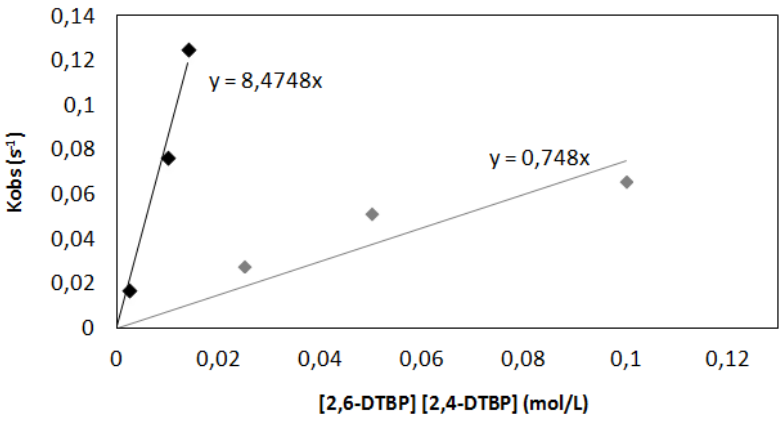

Figure 48. Plots of k_{obs} versus [2,4-DTBP] and [2,6-DTBP] determined for the reaction between **14** and 2,4-DTBP (grey) and for the reaction between **14** and 2,6-DTBP (black) at - 40 °C.

This significant difference in the reaction rate between the two di-tert-butylphenols, suggested that the complex and the substrate need to approach closely to react. As a result, the redox reaction is more likely to proceed though a HAA mechanism rather than an electron transfer (ET) mechanism. Indeed an ET mechanism can be excluded since it can take place at longer distances without a close approach of the reactants. This

hypothesis was also supported by comparing the rate constants measured for the reactions between **14**, **12**, **18** and 2,6-DTBP (Figure 49).

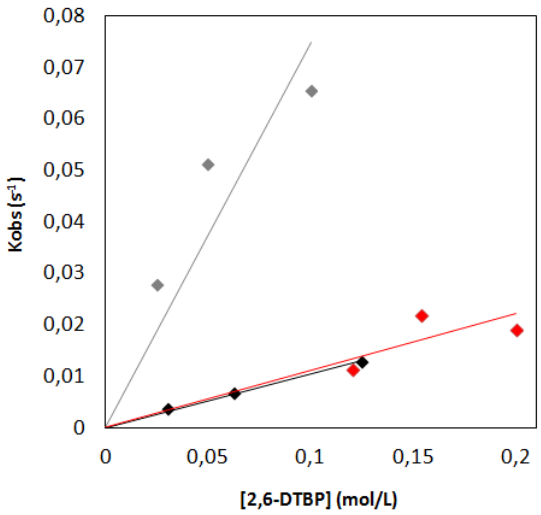

Figure 49. Plots of k_{obs} versus [2,6-DTBP] obtained for the reactions between **14**, **12**, **18** and 2,6-DTBP at - 40 °C . Grey: reaction between **14** and 2,6-DTBP. Black: reaction between **12** and 2,6-DTBP. Red: reaction between **18** and 2,6-DTBP.

The reaction between **14** and 2,6-DTBP was found to be the fastest (k_2 = 0.748 $M^{-1}s^{-1}$) because nitric acid is the strongest acid among those that were employed (pK_a = - 1,4).
As a result nitrate it is the strongest electron-withdrawing group which reduces most the electron density on Ni making it electron poorer and increasing its oxidizing power. **12** and **18,** showed almost the same kinetic constants (k_2 = 0,1033 $M^{-1}s^{-1}$ and k_2 = 0.1103 $M^{-1}s^{-1}$respectively), since they contain anionic ligands (HCO_3^- and CH_3COO^-) arising from acids with very similar values of pK_a (3,6 and 4,76 respectively).
After the HAA reaction, the metal centre should be reduced from Ni(III) to Ni(II) and the ligand should leave the complex forming the corresponding acid such as H_2CO_3 for **12**, HNO_3 for **14** and CH_3COOH for **18**.

2.2.6 Conclusions and future work

The aims of this work were the synthesis and isolation, at low temperature, of Ni(III) complexes containing monodentate oxygen-donor ligands. These compounds are supposed to be very reactive, but their understanding is hampered by the lack of isolated complexes of this type.

During this project we synthesized several Ni(II) complexes, both anionic and neutral, which differ based on the monodentate group in the fourth coordination site. [pyN_2^{R2}] (R= CH_3, iPr) were selected as ideal pincer ligands for the stabilization of the high oxidation states of the metal. In particular, we decided to focus our work exclusively on nickel species featured by [pyN_2^{Me2}]$^{2-}$.

Indeed, only one complex bearing [pyN_2^{iPr2}]$^{2-}$ ([$Ni^{II}(pyN_2^{iPr2})(OH)$]$^-$ (**11**)) was synthesized. The characterization of Ni(II) compounds occurred by ^{1}H NMR, IR and MS spectroscopy.

High-valent Ni(III) complexes were obtained by addition of different one-electron oxidants to the Ni(II) species. The oxidants employed were ‘’magic blue’’ to yield [$Ni^{III}(pyN_2^{Me2})(OCO_2H)$] (**12**), CAN to afford [$Ni^{III}(pyN_2^{Me2})(ONO_2)$] (**14**) and an oxidizing mixtures made up of NaOCl and a carboxylic acid (acetic acid or formic acid) which yielded [$Ni^{III}(pyN_2^{Me2})(OC(O)CH_3)$] (**18**) and [$Ni^{III}(pyN_2^{Me2})(OC(O)H)$] (**25**), respectively.

18 and **25** were obtained in high yield by using, as starting material, their Ni(II) complexes analogue: [$Ni^{II}(pyN_2^{Me2})(OC(O)CH_3)$]$^-$ (**15**) and [$Ni^{II}(pyN_2^{Me2})(OC(O)H)$]$^-$ (**22**) respectively. Indeed, by starting from complex [Ni^{II} (pyN_2^{Me2})(OCO_2H)]$^-$ (**10**), only a partial substitution of the monodentate bicarbonate ligand with the carboxylated anion occurred, and a mixture of the two type of Ni(III) complexes was obtained. Particularly, **15** and **22** were obtained by ligand exchange reaction starting from the neutral complex [$Ni^{II}(pyN_2^{Me2})(CH_3CN)$] (**13**) which contains a easily displaceable acetonitrile group.

Once obtained the Ni(III) species, and characterized by Uv-vis and EPR spectroscopy, we reacted them in situ, with PPh_3 (at – 80 °C) in order to investigate their OAT reactivity, and with 2,6-DTBP (at – 40 °C) in order to probe their HAA reactivity.

During both OAT and HAA reactions, the reduction of the metal centre from Ni(III) to Ni(II), was supposed by the complete disappearance of the two main absorption features of the Ni (III) species in the Uv-vis spectrum. In particular λ_1 = 580 and λ_2 = 900 nm for

14, λ_1 = 520, λ_2 = 750 nm for **18** and λ_1 = 520 and λ_2 = 820 nm for **25**. Moreover, the occurrence of HAA (*i.e* ArOH to ArO·) and OAT (*i.e* PPh_3 to $OPPh_3$) reactions, was confirmed by the presence of the oxidized product in the final reaction mixture, as determined by ^{1}H NMR and MS.

Regarding **14**, it showed to be a competent HAA and OAT agents, and the reaction with a less hindered substrate (2,4-DTBP) was found to be considerably faster than that carried out with 2,6-DTBP at the same temperature. This significant difference, in the reaction rate between the two di-tert-butylphenols, suggested that the redox reaction is more likely to proceed though a HAA mechanism rather than an electron transfer (ET) mechanism.

Regarding **18**, it was capable of hydrogen atom abstraction and that ability was confirm by the addition of 2,6-DTBP and also of 2,6-di-methyl-phenol. The reduction of Ni(III) to Ni (II) occurred also upon the addition of phenol but in this case it was not possible to identify the nature of the product of oxidation of phenol by NMR and mass spectrometry. On the other hand, the addition of PPh_3 to **18** resulted in only slight changes in the Uv-vis spectrum without the complete disappearance of the main two electronic absorption features of the Ni(III) at the end of the reaction. According to this result, it was supposed the occurrence of a ligand exchange reaction with PPh_3 instead of the of the expected redox reaction.

By comparing the values of the second-order reaction rate for the HAA reactions performed with 2,6-DTBP, **14** and was found to be the fastest (k_2 = 0.748 $M^{-1}s^{-1}$). Indeed, since nitrate is a weaker electron-donor group compared to the bicarbonate and acetate, it reduces most the electron density on nickel increasing its oxidizing power.

Regarding the oxygen atom transfer reactions performed by adding PPh_3, **12** was found to be the most reactive among the other Ni(III)species. According to this result, for **12** we supposed a concerted mechanism (OAT). This proposed concertated mechanism, was also supported by the fact that **18** and **25** containing a carboxylate ligand instead of a bicarbonate, are not reactive towards PPh_3.

Finally, since **14** was found to be less reactive compared to **12** and more reactive compared to **18** and **25,** we thought that the reaction between **14** and PPh_3 could have followed either an OAT or an ET mechanism.

Overall, the results obtained for the oxygen atom transfer reactions, led us to conclude that the mechanism, in this case, could depend on the nature of the ligand binding the metal centre.

In the future, the work herein presented might be extended in different ways. First, the structure of the substrates (PPh_3 or 2,6-DTBP) could be modified by binding different electron withdrawing or electron donor groups. In this way the ability of the substrate to be oxidized can be changed, and the results obtained could provide further insight into the reaction mechanism.

Preliminary tests carried out using the Ni(III) complex **18** at 25 °C confirmed its reactivity towards hardly oxidizable substrates such as fluorene, cyclohexadiene, diidroantracene, thioanisole, toluene, ethylbenzene, cyclohexane. Oxidation of hydrocarbon substrates could be investigated by using this complex.

3. Experimental

3.1 General

3.1.1 Physical methods

Electronic absorption spectra were recorded on a HewlettPackard (Agilent) 8453 diode array spectrophotometer (190-1100 nm range) in quartz cuvettes cooled using a liquid nitrogen cooled cryostat from Unisoku Scientific Instruments (Osaka, Japan). ^{1}H and ^{31}P NMR analyses were performed on a Bruker Avance III 400 MHz instrument. GC-MS was performed using a GCT Premier Micromass time of flight mass spectrometer (tof). SI mass spectra were acquired using a Micromass time of flight spectrometer (tof), interfaced to a Waters 2690 HPLC. EPR spectra were recorded on a Magnetech Miniscope MS2000 instrument, with liquid nitrogen cooling.

3.1.2 Materials

All reactions with air-sensitive materials were conducted under an inert atmosphere using either standard Schlenk techniques or a nitrogen atmosphere glove box. All reagents and solvents were purchased from commercial sources and used as received, unless otherwise stated. Anhydrous DMF and acetonitrile were purchased and used without further purification. Anhydrous THF and diethyl ether were dispensed through an Innovative Technology PureSolv EN solvent purification system and deoxygenated by purging with argon. Acetone was dried over magnesium sulfate, then over 4 Å molecular sieves, distilled and deoxygenated by purging with argon.

3.2 Synthesis of $H_2pyN_2^{Me2}$ and $[Ni(CH_3CN)_6](OTf)_2$

3.2.1 Synthesis of $H_2pyN_2^{Me2}$

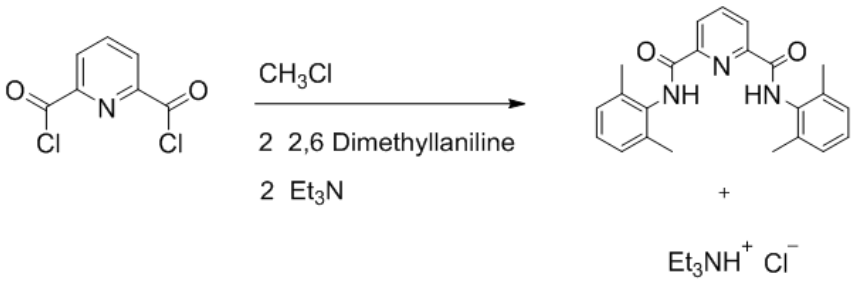

Figure 50. Synthesis of $H_2pyN_2^{Me2}$

Pyridine-2,6-dicarbonyl chloride (8 g , 0.039 mol) was dissolved in CH_3Cl (150 mL); 2,6 dimethylaniline (9.50 mL, 0.078 mol) and triethylamine (10.60 mL, 0.078 mol) were added to the solution and the reaction was stirred for 5 h at room temperature (Figure 50). $[Et_3N][Cl]$ was removed from the reaction mixture by washing with an aqueous solution of $HCl/NaHCO_3$. The final product was obtained as white solid in high yield after evaporation of the solvent. (11.20 g, 77 %)

$H_2pyN_2^{Me2}$: δ_H **(400 MHz, CDCl3)** 2.27 (12H, s, Ar-CH_3), 7.10-7.18 (6H, m, 3, 4, 5-Ar), 8.14 (1H, t, *J* = 7.9 Hz, 4-py), 8.51 (2H, d, *J* = 7.9 Hz, 3, 5-py), 9.17 (2H, s, H-N)

3.2.2 Synthesis of $[Ni(CH_3CN)_6][OTf]_2$

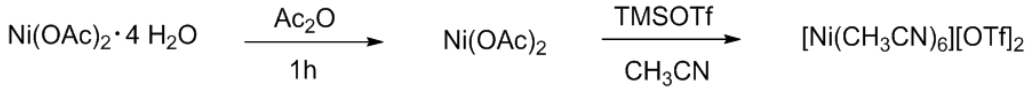

Figure 51. Synthesis of $[Ni(CH_3CN)_6][OTf]_2$

$Ni(OAc)_2 \cdot 4H_2O$ was covered with Ac_2O and brought to reflux for 1 h (Figure 51). After the reaction the solution was cooled down and put in the freezer. After the solidification, Ac_2O was allowed to melt, then $Ni(OAc)_2$ filtered and washed with hexane and diethyl ether. The so obtained anhydrous $Ni(OAc)_2$ anydrous (500 mg, 1 eq) was reacted with CH_3CN (3 mL) and TMSOTf (1.02 mL, 5.66 mol, 2 eq) for 2 hours at room temperature. After the reaction diethyl ether (10 mL) was added and the precipitate obtained was filtered.

$[Ni(CH_3CN)_6][OTf]_2$: IR (KBr): 2949 cm^{-1}(CH); 2301 cm^{-1}(C≡N); 1029 cm^{-1} (SO_3^-)

3.3 Synthesis of Ni (II) complexes

3.3.1 Synthesis of $[Et_4N][Ni^{II}(pyN_2^{Me2})(OH)]$ (8)

$H_2pyN_2^{Me2}$ (0.5 g, 1.33 mmol) was completely dissolved in THF (5 mL), then $[Ni(CH_3CN)_6][OTf]_2$ (0.802 mg, 1.33 mmol) and $[Et_4N][OH]$ (25% in methanol, 2.66 mL, 3.99 mmol) were added and the mixture was stirred for 2 h to give a red suspension.
A second equal portion of $[Et_4N][OH]$ was added, and the mixture was stirred for 10 h to afford a deep red solution and some sticky precipitate. Addition of hexane (20 mL) to the sticky precipitate resulted in an oil, which was stirred in anhydrous diethyl ether (10 mL) for 30 minutes to give a red powder. In order to remove $[Et_4N][OTf]$ from the powder, the latter was dissolved in a small volume of DMF (2 mL) and then diethyl ether was diffused slowly. This crystallization process yielded a red crystalline solid (138 mg, 60%). To improve the removal of the salt a washing with toluene as well as a

crystallization from methanol and THF were tried, but both processes were found to be less efficient compared to the first. The nature of the complex was confirmed by ^{1}H NMR, UV-vis and ATR-FTIR spectroscopies, and its stability in acetone solutions verified by ^{1}H NMR.

[Et$_4$N][Ni^{II}(pyN_2^{Me2})(OH)] (8): δ_H **(400 MHz, [D$_6$]acetone)** -4.89 (1H, s, O*H*), 1.35 (12H, t, *J* = 6.8 Hz, NCH$_2$C*H*$_3$), 2.50 (12H, s, ArC*H*$_3$), 3.45 (8H, q, *J* = 6.8 Hz, NC*H*$_2$CH$_3$), 6.77 (2H, t, *J* = 7.2 Hz, 4-Ar), 6.85 (4H, d, *J* = 7.2 Hz, 3,5-Ar), 7.49 (2H, d, *J* = 7.7 Hz, 3,5-py), 8.00 (1H, t, *J* = 7.2 Hz, 4-py)**; IR** (KBr): *ν*OH 3594 cm^{-1}; λ_{max} **(DMF)/nm :** 411 (ε/dm^3 mol^{-1}cm^{-1} 5500), 483 (sh, 2600).

3.3.2 Synthesis of [Et$_4$N][Ni^{II}(pyN_2^{Me2})(OCO$_2$H)] (10)

A solution of [Et$_4$N][Ni^{II} (pyN_2^{Me2})(OH)] (**8**) (23 mg, 0.040 mmol) in acetone (2 mL) was bubbled with carbon dioxide for 15 min. Diffusion of ether into the red solution gave the product as orange-red crystals (21 mg, 85%).

[Et$_4$N][Ni^{II}(pyN_2^{Me2})(OCO$_2$H)] (10): δ_H (400 MHz, [D$_6$]acetone) 1.39 (12H, t, *J* = 7.0 Hz, NCH$_2$C*H*$_3$), 2.52 (12H, s, ArC*H*$_3$), 3.42 (8H, q, *J* = 7.0 Hz, NC*H*$_2$CH$_3$), 6.77 (2H, t, *J* = 6.7 Hz, 4-Ar), 6.85 (4H, d, *J* = 6.7 Hz, 3,5-Ar), 7.50 (2H, d, *J* = 7.3 Hz, 3,5-py), 8.09 (1H, t, *J* = 7.3 Hz, 4-py).

3.3.3 Synthesis of $[Et_4N][Ni^{II}(pyN_2^{iPr2})(OH)]$ (11)

3.3.3.1 Synthesis of $[Et_4N][Ni^{II}(pyN_2^{iPr2})(OH)]$ (11) from $[Ni(CH_3CN)_6][OTf]_2$

$H_2pyN_2^{iPr2}$ (500 mg, 1.02 mmol) was dissolved in THF (10 mL) and sodium hydride (60% dispersion in mineral oil, 82.3 mg, 2.04 mmol, 2 eq) was added. After ½ hours of stirring, bubbling had ceased and the solution had assumed a yellow tinge. $[Ni(CH_3CN)_6][OTf]_2$ (620 mg, 1.02 mmol, 1 eq) was added causing the solution to immediately turn dark red-brown. After ½ hours of stirring, the solvent was removed in vacuum and the remaining solid extracted into 10 mL of CH_2Cl_2. Diffusion of diethyl ether into this solution afforded the product $[Ni^{II}(pyN_2^{iPr2})(CH_3CN)]$ (**9**) as blocky red crystals (220 mg, 37%). Afterwards, **9** was reacted with 1 equivalent of $[Et_4N][OH]$ yielding to the final product $[Et_4N][Ni^{II}(pyN_2^{iPr2})(OH)]$ (**11**).

$[Ni^{II}(pyN_2^{iPr2})(CH_3CN)]$(9): δ_H (400 MHz, CDCl3) 1.26 (3H, s, C*H*$_3$CN), 1.28 (12H, d, *J* = 6.5 Hz, CH(C*H*$_3$)$_2$), 1.44 (12H, d, *J* = 6.5 Hz, CH(C*H*$_3$)$_2$), 3.82 (4H, m, C*H*(CH$_3$)$_2$), 7.02–7.18 (6H, m, 3, 4, 5,-Ar*H*), 7.77 (2H, d, *J* = 7.7 Hz, 3,5-py), 8.08 (1H, t, *J* = 7.7 Hz, 4-py).

$[Et_4N][Ni^{II}(pyN_2^{iPr2})(OH)]$ (11): δ_H (400 MHz, CDCl3) -5.19 (1H, s, O*H*), 1.17 (12H, d, *J* = 17 Hz, CH(C*H*$_3$)$_2$), 1.35 (12H, t, *J* = 6.8 Hz, NCH$_2$C*H*$_3$), 1.25-1.35 (15H, m, CH(C*H*$_3$)$_2$ and C*H*$_3$CN), 3.45 (8H, q, *J* = 6.8 Hz, NC*H*$_2$CH$_3$) 3.82 (4H, m, C*H*(CH$_3$)$_2$), 6.78–6.90 (6H, m, 3, 4, 5-Ar*H*), 7.58 (2H, d, *J* = 7.8 Hz, 3,5-py), 7.85 (1H, t, *J* = 7.8 Hz, 4-py).

3.3.3.2 Synthesis of $[Et_4N][Ni^{II}(pyN_2^{iPr2})(OH)]$ (11) from $Ni(OAc)_2 \cdot 4H_2O$

$H_2pyN_2^{iPr2}$ (500 mg, 1.02 mmol) was dissolved in THF (10 mL) and sodium hydride (60% dispersion in mineral oil, 82.3 mg, 2.04 mmol, 2 eq) was added. After ½ hours of stirring, bubbling had ceased and the solution had assumed a yellow tinge. $Ni(OAc)_2 \cdot 4H_2O$ (255 mg, 1.02 mmol, 1 eq) was added causing the solution to immediately turn green, and finally dark red-brown. Afterwards, CH_3CN was added (20 mL) and the reaction mixture was let stirring overnight. The day after, THF was evaporated and the ^1H NMR of the mixture showed an excess of 30 % of ligand which was removed by washing with toluene and 1 equivalent of $[Et_4N][OH]$ was added to the mixture to obtain the final product. The product was obtained in traces.

3.3.3.3 Synthesis of $[Et_4N][Ni^{II}(pyN_2^{iPr2})(OH)]$ (11) from $Ni(OTs)_2$

$H_2pyN_2^{iPr2}$ (500 mg, 1.02 mmol) was dissolved in THF (10 mL) and sodium hydride (60% dispersion in mineral oil, 82.3 mg, 2.04 mmol, 2 eq) was added. After ½ hours of stirring, bubbling had ceased and the solution had assumed a yellow tinge. Addition of $Ni(OTs)_2$ (483 mg, 1.02 mmol, 1 eq) was performed, causing the solution to immediately turn dark red-brown, followed by that of CH_3CN (20 mL), and the reaction mixture was let stirring overnight. The day after, THF was evaporated and an extraction DCM/H_2O was carried out in order to remove NaOTs from the reaction mixture.^1H NMR spectrum showed an excess of ligand which was removed by washing with toluene.

Finally 1 eq of $[Et_4N][OH]$ was added to the mixture. This process yielded an orange powder (43 mg, 24 %).

3.3.4 Synthesis of [$Ni^{II}(pyN_2^{Me2})(CH_3CN)$] (13)

3.3.4.1 Synthesis of [$Ni^{II}(pyN_2^{Me2})(CH_3CN)$] (13) from $Ni(OTs)_2$ using THF as solvent and CH_3CN as reagent

$H_2pyN_2^{Me2}$ (500 mg, 1.02 mmol) was dissolved in THF (15 mL) and sodium hydride (60% dispersion in mineral oil, 42 mg, 1.03 mmol, 2 eq) was added. After ½ hours of stirring, bubbling had ceased and the solution had assumed a light brown tinge. $Ni(OTs)_2$ (624 mg, 1.02 mmol, 1 eq) was added causing the solution to immediately turn dark red-brown. Finally CH_3CN was added (20 mL), and the reaction mixture was let stirring overnight. The next day, THF was evaporated and a DCM/H_2O extraction was carried out in order to remove NaOTs from the mixture. The solid product obtained from both the organic phase and aqueous phase was analysed by ^1H NMR. The ^1H NMR spectrum of the organic phase showed the presence of free ligand, and in the ^1H NMR spectrum of the aqueous phase the species $Na[Ni^{II}(pyN_2^{Me2})(OTs)]$ (**17**) was present instead of the expected product $[Ni^{II}(pyN_2^{Me2})(CH_3CN)]$(**13**).

$Na[Ni^{II}(pyN_2^{Me2})(OTs)]$ (17): δ_H (400 MHz, CD_3OD) 1.16 (12H, t, J = 7.2 Hz, $NCH_2\mathit{CH_3}$), 2.35 (3H, s, $\mathit{CH_3}$-Ar-Tos), 2.52 (12H, s, $ArC\mathit{H_3}$), 3.58 (8H, q, J = 7.2 Hz, $N\mathit{CH_2}CH_3$), 6.88 (6H, m, 3, 4, 5-Ar), 7.21 (2H, d, J = 7.6 Hz, 2, 3-Ar-Tos), 7.59 (2H, d, J = 7.8 Hz, 3, 5-py), 7.68 (2H, d, J = 7.9 Hz, 5,6-Ar-Tos), 8.10 (1H, t, J = 7.7 Hz 4-py).

3.3.4.2 Synthesis of [$Ni^{II}(pyN_2^{Me2})(CH_3CN)$] (13) from $Ni(OTs)_2$ dissolving the ligand in CH_3CN

$H_2pyN_2^{Me2}$ (500 mg, 1.3 mmol) was dissolved in acetonitrile (15 mL) and sodium hydride (60% dispersion in mineral oil, 106 mg, 2.6 mmol, 2 eq) was added. Upon the addition of $Ni(OTs)_2$ (624 mg, 1.3 mmol, 1 eq), the solution turned immediately dark red-brown and the reaction mixture was let stirring overnight. The day after, CH_3CN was evaporated by Rotavapor and the solid obtained was dissolved in DCM (50 mL) for the removal of NaOTs. After that, the solution was filtered and both solid and liquid phase

were analysed by ^{1}H NMR and IR. Both spectra confirmed the presence of $Na[Ni^{II}(pyN_2^{Me2})(OTs)]$ (**17**) instead of $[Ni^{II}(pyN_2^{Me2})(CH_3CN)]$ (**13**).

$Na[Ni^{II}(pyN_2^{Me2})(OTs)]$ (17): IR (KBr) *ν* C=O 1604 cm^{-1} , *ν* C-H (around) 3000 cm^{-1} , *ν* Tosylate : 1202cm^{-1} 1045cm^{-1} 563cm^{-1}

3.3.4.3 Synthesis of $[Ni^{II}(pyN_2^{Me2})(CH_3CN)]$ (13) from $[Ni(CH_3CN)_6][OTf]_2$ dissolving the ligand in CH_3CN

$H_2pyN_2^{Me2}$ (500 mg, 1.3 mmol) was dissolved in acetonitrile (15 mL) and sodium hydride (60% dispersion in mineral oil, 106 mg, 2.6 mmol, 2 eq) was added. $[Ni(CH_3CN)_6][OTf]_2$ (802 mg, 1.3 mmol, 1 eq) was added causing the solution to immediately turn dark red-brown and the reaction mixture was let stirring overnight. The removal of sodium salt was carried out by extraction with DCM (50 mL). The mixture obtained was filtered and the expected product $[Ni^{II}(pyN_2^{Me2})(CH_3CN)]$ was obtained (0.245 g, 15 %).

$[Ni^{II}(pyN_2^{Me2})(CH_3CN)]$ (13): δ_H (400 MHz, $CDCl_3$) 1.29 (3H, s, CH_3CN), 2.49 (12H, s, Ar*CH*$_3$), 6.94 (6H, m, 3, 4, 5-Ar), 7.79 (2H, d, J = 7,7 Hz, 3,5-py), 8.06 (1H, t, J = 7,8 Hz, 4-py); **ESI-MS (Direct injection, m/z)** Found (positive mode): 471.1331 ($[M+H]^+$, $C_{25}H_{25}N_4NiO_2^+$); **IR (KBr):** 2309 cm^{-1}(C≡N); 1631 cm^{-1}, 1606 cm^{-1}(C=O); 2971 cm^{-1}, 2912 cm^{-1} (CH); **λ_{max} (CH_3CN)/nm :** 333 (ε/dm^3 $mol^{-1}cm^{-1}$ 1700), 430sh (90).

3.3.5 Ligand exchange reaction of [$Ni^{II}(pyN_2^{Me2})(CH_3CN)$] (13)

Three ligand exchange reactions were carried out by reacting [$Ni^{II}(pyN_2^{Me2})(CH_3CN)$] (**13**) with [$Et_4N$][$OC(O)CH_3$], [$Et_4N$][Cl], and [$Et_4N$][OC(O)H] in a ratio 1:1 at room temperature. The complex and all the reagents were dissolved in acetonitrile (except for [Et_4N][$OC(O)CH_3$] that was dissolved in methanol). After the reaction, the final mixture was crystallized with diethyl ether and the solid analysed by ^{1}H NMR, IR, MS.

[Et_4N][$Ni^{II}(pyN_2^{Me2})(OC(O)CH_3)$] (15): δ_H (400 MHz, CD_2Cl_2): 0.76 (3H, s, CH_3Ac), 1.08 (12H, t, J = 7.2 Hz, NCH_2CH_3), 2.57 (12H, s, ArCH_3), 2.89 (8H, q, J = 7.2 Hz, NCH_2CH_3), 6.82 (6H, m, 3, 4, 5-Ar), 7.51 (2H, d, J = 7.9 Hz, 3, 5-py), 7.88 (1H, t, J = 7.9 Hz, 4-py); **ESI-MS (Direct injection, m/z)** Found (negative mode): 488.1128 ([M^-] $C_{25}H_{24}N_3NiO_4^-$)**; IR (KBr):** 2911 cm^{-1}, 2939 cm^{-1} (CH), 1606 cm^{-1} (C=O); λ_{max} **(Acetone)/nm:** 380 (ε/dm^3 $mol^{-1}cm^{-1}$5500), 475 (sh, 1500).

[Et_4N][$Ni^{II}(pyN_2^{Me2})(Cl)$] (20): δ_H (400 MHz, CD_2Cl_2) 1.11 (12H, t, J = 7.2 Hz, NCH_2CH_3), 2.43 (12H, s, ArCH_3), 3.04 (8H, q, J = 7.3 Hz, NCH_2CH_3), 6.69 (6H, m, 3, 4, 5-Ar) 7.62 (2H, d, J = 7.7 Hz, 3, 5-py), 7.92 (1H, t, J = 7.6 Hz, 4-py); **ESI-MS (Direct injection, m/z)** Found (negative mode): 464.0680 ([M^-], $C_{23}H_{21}ClN_3NiO_2^-$); **IR (KBr):** 2982 cm^{-1} (CH), 1603 cm^{-1}(C=O); λ_{max} **(Acetone)/nm:** 390 (ε/dm^3 $mol^{-1}cm^{-1}$ 5500), 460 (1400), 500 (1000).

[Et_4N][$Ni^{II}(pyN_2^{Me2})(OC(O)H)$] (25): δ_H (400 MHz, CD_2Cl_2): 1.87 (12H, t, J = 7.2 Hz, NCH_2CH_3), 2.54 (12H, s, ArCH_3), 2.81 (8H, q, J = 7.2 Hz, NCH_2CH_3), 6.83 (6H, m, 3, 4, 5-Ar), 7.10 (1H, s, -OC(O)*H*), 7.56 (2H, d, , J = 7.6 Hz, 3, 5-py), 7.90 (1H, t, J = 7.7 Hz, 4-py); **IR (KBr):** 2980 cm^{-1} (CH), 1613 cm^{-1} (C=O); **ESI-MS (Direct injection, m/z)** Found (negative mode): 474.0982 ([M^-] $C_{25}H_{22}N_3NiO_4^-$); λ_{max} **(Acetone)/nm :** 380 (ε/dm^3 $mol^{-1}cm^{-1}$5500), 475 (sh, 1500).

3.4 Reactivity studies

3.4.1 General procedure for the oxidation of Ni(II) species

Solutions of Ni(II) complexes were prepared in acetone (0.2 -0.5 mM depending on the compound). Oxidations were conducted on 2 mL of solution in cryostated quartz cuvettes at -80°C (or -40°C) under continuous stirring. Oxidants were added as concentrated solutions; Magic Blue (15 mM in CH_3CN) was used in stoichiometric amounts; excess CAN was dissolved in methanol (1 M); the oxidizing mixture NaOCl/carboxylic acid was used in a ratio 1:10 . The reactions were monitored by the changes in the UV-vis spectra and all solutions were freshly prepared at least once per day. The reaction mixtures were diluted with methanol for MS analyses, or the solvent was removed in vacuo for NMR analysis.

3.4.2 General procedure for the EPR analyses of cold solutions

Samples for EPR analysis were prepared by transferring an aliquot of the desired solution, from the cuvette, *via* a pre-cooled pipette, into a pre-cooled quartz EPR tube and immediately freezing it in liquid nitrogen. All EPR spectra were recorded at 113 K, 9.387 GHz, 31.6 W microwave power, with a 300 mT field sweep in 60 s, and 0.5 mT field modulation amplitude. Integration, simulation and fitting were executed with Matlab and the easySpin computational package. Quantification of the concentration of spins in the sample was determined by comparison of the double integral of the signal to that of a frozen 0.4 mM acetone solution of (2,2,6,6-tetramethyl-piperidin-1-yl)oxyl (TEMPO), measured under the same conditions.

3.4.3 Determination of the rate constants

Reactions were executed with 7 to 500 equivalents of substrate to ensure pseudo-first order conditions. The second-order rate constant were determined from the linear dependence of the pseudo-first order constant on substrate concentration. Values for the

observed k_{obs} were obtained by fitting the decay of the absorbance at the main electronic absorption features during a reaction as an exponential. The average from repeated experiments was utilized for the determination of k_2.

4. References

[1] M. V. Doble, A. C. C.Ward, P. J. Deuss, A. G. Jarvis and P. C. J. Kamer, *Bioorg. Med. Chem.*, 2014, 22, 5657–5677.

[2] H. Arakawa, M. Aresta, J. N. Armor, M. A. Barteau, E. J. Beckman, A. T. Bell, J. E. Bercaw, C. Creutz, E. Dinjus, D. A. Dixon, K. Domen, D. L. DuBois, J. Eckert, E. Fujita, D. H. Gibson,W. A. Goddard, D.W. Goodman, J. Keller, G. J. Kubas, H. H. Kung, J. E. Lyons, L. E. Manzer, T. J.Marks, K. Morokuma, K. M. Nicholas, R. Periana, L. Que, J. Rostrup-Nielson, W. M. H. Sachtler, L. D. Schmidt, A. Sen, G. A. Somorjai, P. C. Stair, B. R. Stults and W. Tumas, *Chem. Rev.*, 2001, 101, 953–996.

[3] J.A. Labinger and J.E. Bercaw, Nature, 2002, 417, 507-514.

[4] L. Que and W. B. Tolman, *Nature*, 2008, 455, 333–340.

[5] K. Ray, F. F. Pfaff, B. Wang and W. Nam, *J. Am. Chem. Soc.*, 2014.

[6] D. E. Torres Pazmino, M. Winkler, A. Glieder and M. W. Fraaije, *J. Biotechnol.*, 2010, 146, 9–24.

[7] M. Sono, M. P. Roach, E. D. Coulter and J. H. Dawson, *Chem. Rev.*, 1996, 96, 2841–2888.

[8] B. Meunier, S. P. de Visser and S. Shaik, *Chem. Rev.*, 2004, 104, 3947–3980.

[9] W. Nam, Y.-M. Lee and S. Fukuzumi, *Acc. Chem. Res.*, 2014, 47, 1146–1154.

[10] S. Hammes-Schiffer and A. A. Stuchebrukhov, *Chem. Rev.*, 2010, 110, 6939–6960.

[11] J. Zurek, N. Foloppe, J.N. Harvey and A. J. Mulholland, *Org. Biomol. Chem.*, 2006, 4, 3931–3937

[12] J. T. Groves, R. C. Haushalter, M. Nakamura, T. E. Nemo and B. J. Evans, *J. Am. Chem. Soc.*, 1981, 103, 2884–2886.

[13] J. E. Penner-Hahn, T. J. McMurry, M. Renner, L. Latos-Grazynsky, K. S. Eble, I. M. Davis, A. L.Balch, J. T. Groves, J. H. Dawson and K. O. Hodgson, *J. Biol. Chem.*, 1983, 258, 12761–12764.

[14] J. E. Penner-Hahn, K. Smith Eble, T. J.McMurry, M. Renner, A. L. Balch, J. T. Groves, J. H. Dawson and K. O. Hodgson, *J. Am. Chem. Soc.*, 1986, 108, 7819–7825.

[15] L. Que, *Acc. Chem. Res.*, 2007, 40, 493–500.

[16] W. Nam, *Acc. Chem. Res.*, 2007, 40, 522–531.

[17] A. R. McDonald and L. Que, *Coord. Chem. Rev.*, 2013, 257, 414–428.

[18] A. W. Pierpont and T. R. Cundari, *Inorg. Chem.*, 2010, 49, 2038–2046.

[19] C. E. MacBeth, *Science*, 2000, 289, 938–941.

[20] T. R. Cundari, R. R. Conry, E. Spaltenstein, S. C. Critchlow, K. A. Hall, S. K. Tahmassebi and J. M.Mayer, *Organometallics*, 1994, 13, 322–331.

[21] S. Hong, F. F. Pfaff, E. Kwon, Y. Wang, M.-S. Seo, E. Bill, K. Ray and W. Nam, *Angew. Chem. Int.Ed.*, 2014, 53, 10493–10407.

[22] F. F. Pfaff, F. Heims, S. Kundu, S. Mebs and K. Ray, *Chem. Commun.*, 2012, 48, 3730–3732.

[23] P. J. Donoghue, J. Tehranchi, C. J. Cramer, R. Sarangi, E. I. Solomon and W. B. Tolman, *J. Am.Chem. Soc.*, 2011, 133, 17602–17605.

[24] E. Poverenov, I. Efremenko, A. I. Frenkel, Y. Ben-David, L. J. W. Shimon, G. Leitus, L. Konstantinovski, J. M. L. Martin and D. Milstein, *Nature*, 2008, 455, 1093–1096.

[25] R. P. Hausinger, *J. Biol Inorg. Chem.*,1997, 2, 279–286

[26] Roat-Malone, Bioinorganic Chemistry: A Short Course, Wiley-Interscience, 2002, ISBN 0-471-15976-X

[27] Y. Li and D. B. Zamble, *Chem. Rev.*, 2009, 109, 4617–4643.

[28] N. Yahata, T. Saitoh, Y. Takayama, K. Ozawa, H. Ogata, Y. Higuchi and H. Akutsu , *Biochemistry*, 2006, 45, 1653–1662

[29] J.L. Craft, Y.C Horng, S.W. Ragsdale, and Thomas C. Brunold, J. Am. Chem. Soc., 2004, 126, 4068–4069.

[30] SW Ragsdale.*J. Biol. Chem.*, 2009, 284, 18571-18575.

[31] P. Pirovano, E. R. Farquhar, M. Swart, A. J. Fitzpatrick, G. G. Morgan and A. R. McDonald, *Chem.Eur. J.*, 2015, 21, 3785-3790.

[32] P. J. Chmielewski and L. Latos-Grazynsky, *Inorg. Chem.*, 1997, 36, 840–845.

[33] S. Hikichi, M. Yoshizawa, Y. Sasakura, M. Akita and Y. Moro-oka, *J. Am. Chem. Soc.*, 1998, 120, 10567–10568.

[34] S. Itoh, H. Bandoh, S. Nagatomo, T. Kitagawa and S. Fukuzumi, *J. Am. Chem. Soc.*, 1999, 121, 8945–8946.

[35] K. Shiren, S. Ogo, S. Fujinami, H. Hayashi, M. Suzuki, A. Uehara, Y. Watanabe and Y. Moro-oka, *J. Am. Chem. Soc.*, 2000, 122, 254–262.

[36] S. Itoh, H. Bandoh, M. Nakagawa, S. Nagatomo, T. Kitagawa, K. D. Karlin and S. Fukuzumi, *J. Am. Chem. Soc.*, 2001, 123, 11168–11178.

[37] R. Schenker, B. S. Mandimutsira, C. G. Riordan and T. C. Brunold, *J. Am. Chem. Soc.*, 2002, 124, 13842–13855.

[38] K. Fujita, R. Schenker, W. Gu, T. C. Brunold, S. P. Cramer and C. G. Riordan, *Inorg. Chem.*, 2004, 43, 3324–3326.

[39] S. Kundu, F. F. Pfaff, E. Miceli, I. Zaharieva, C. Herwig, S. Yao, E. R. Farquhar, U. Kuhlmann, E. Bill, P. Hild

[40] S. A. Jacobs and D. W. Margerum, *Inorg. Chem.*, 1984, 23, 1195–1201.

[41] H. J. Kruger, G. Peng and R. H. Holm, *Inorg. Chem.*, 1991, 30, 734–742.

[42] F. V. Lovecchio, E. S. Gore and D. H. Busch, *J. Am. Chem. Soc.*, 1974, 96, 3109–3118.

[43] R. Haines and A. McAuley, *Coord. Chem. Rev.*, 1981, 39, 77–119.

[44] J. N. Stuart, A. L. Goerges and J. M. Zaleski, *Inorg. Chem.*, 2000, 39, 5976–5984.

[45] P. J. Alonso, L. R. Falvello, J. Fornies, A. Martin, B. Menjon and G. Rodriguez, *Chem. Commun.*, 1997, 2, 503–504.

[46] T. J. Collins, T. R. Nichols and E. S. Uffelman, *J. Am. Chem. Soc.*, 1991, 113, 4708–4709.

[47] X. Ottenwaelder, R. Ruiz-Garcia, G. Blondin, R. Carasco, J. Cano, D. Lexa, Y. Journaux and A. Aukauloo, *Chem. Commun.*, 2004, 504–505.